

OCIT

018193



The University Of Alabama In Huntsville

Solar Thermal Concept Evaluation

Marshall Space Flight Center

REPORT DOCUMENTATION PAGE

Form Approved

OMB No. 0704 0188

Public reporting burden for this collection of information is estimated to average 1 hour per response, including the time for reviewing instructions, searching existing data sources, gathering and maintaining the data needed, and completing and reviewing the collection of information. Send comments regarding this burden estimate or any other aspect of this collection of information, including suggestions for reducing the burden, to Washing Headquarters Services, Directorate for Information Operations and Reports, 1215 Jefferson Davis Highway, Suite 1204, Arlington, VA 22202-4302, and to the Office of Management and Budget, Paperwork Reduction Project (0704-0138), Washington, DC 20503

1. AGENCY USE ONLY (leave blank)		2. REPORT DATE 31 August 95		3. REPORT TYPE AND DATES COVERED Final Report (4 March 94 - 4 July 95)	
4. TITLE AND SUBTITLE Solar Thermal Concept Evaluation Final Technical Report				5. FUNDING NUMBERS H-17654D	
6. AUTHOR(S) Joseph A. Bonometti					
7. PERFORMING ORGANIZATION NAME(S) AND ADDRESS(ES) Propulsion Research Center University of Alabama in Huntsville Huntsville, AL 35899				8. PERFORMING ORGANIZATION REPORT NUMBER	
9. SPONSORING/MONITORING AGENCY NAME(S) AND ADDRESS(ES) NASA Attn: Lott W. Brantley, Jr. PR41 George C. Marshall Space Flight Center MSEC, AL 35812				10. SPONSORING/MONITORING AGENCY REPORT NUMBER	
11. SUPPLEMENTARY NOTES					
12a. DISTRIBUTION/AVAILABILITY STATEMENT				12b. DISTRIBUTION CODE	
13. ABSTRACT (Maximum 200 words) <p>Concentrated solar thermal energy can be utilized in a variety of high temperature applications for both terrestrial and space environments. In each application, knowledge of the collector and absorber's heat exchange interaction is required. To understand this coupled mechanism, various concentrator types and geometries, as well as, their relationship to the physical absorber mechanics were investigated.</p> <p>To conduct experimental tests, various parts of a 5,000 watt, thermal concentrator, facility were made and evaluated. This was in anticipation of a larger NASA facility proposed for construction. Although much of the work centered on solar thermal propulsion for an upper stage (less than one pound thrust range), the information generated and the facility's capabilities are applicable to material processing, power generation and similar uses.</p> <p>The numerical calculations used to design the laboratory mirror and the procedure for evaluating other solar collectors are presented here. The mirror design is based on a hexagonal faceted system, which uses a spherical approximation to the parabolic surface. The work began with a few two dimensional estimates and continued with a full, three dimensional, numerical algorithm written in FORTRAN code. This was compared to a full geometry, ray trace program, BEAM 4, which optimizes the curvatures, based on purely optical considerations.</p> <p>Founded on numerical results, the characteristics of a faceted concentrator were construed. The numerical methodologies themselves were evaluated and categorized. As a result, the three-dimensional FORTRAN code was the method chosen to construct the mirrors, due to its overall accuracy and superior results to the ray trace program. This information is being used to fabricate and subsequently, laser map the actual mirror surfaces.</p> <p>Evaluation of concentrator mirrors, thermal applications and scaling the results of the 10 foot diameter mirror to a much larger concentrator, were studied. Evaluations, recommendations and pit falls regarding the structure, materials and facility design are presented.</p>					
14. SUBJECT TERMS Solar thermal mirrors Spherical approximation to parabolic curve Solar thermal propulsion				15. NUMBER OF PAGES 43	
				16. PRICE CODE	
17. SECURITY CLASSIFICATION OF REPORT UNCLASSIFIED		18. SECURITY CLASSIFICATION OF THIS PAGE UNCLASSIFIED		19. SECURITY CLASSIFICATION OF ABSTRACT UNCLASSIFIED	
				20. LIMITATION OF ABSTRACT UL	

UAH Propulsion Research Center

SOLAR THERMAL CONCEPT EVALUATION

Final Technical Report

NASA/Marshall Space Flight Center
NASA contract number H-17654D

Prepared by

Joseph A. Bonometti

Submitted to:

Lott W. Brantley PS05
Marshall Space Flight Center, AL 35812

Dr. Clark W. Hawk
Principal Investigator
Propulsion Research Center
The University of Alabama in Huntsville

August 31, 1995

Abstract

Concentrated solar thermal energy can be utilized in a variety of high temperature applications for both terrestrial and space environments. In each application, knowledge of the collector and absorber's heat exchange interaction is required. To understand this coupled mechanism, various concentrator types and geometries, as well as, their relationship to the physical absorber mechanics were investigated.

To conduct experimental tests, various parts of a 5,000 watt, thermal concentrator, facility were made and evaluated. This was in anticipation of a larger NASA facility proposed for construction. Although much of the work centered on solar thermal propulsion for an upper stage (less than one pound thrust range), the information generated and the facility's capabilities are applicable to material processing, power generation and similar uses.

The numerical calculations used to design the laboratory mirror and the procedure for evaluating other solar collectors are presented here. The mirror design is based on a hexagonal faceted system, which uses a spherical approximation to the parabolic surface. The work began with a few two dimensional estimates and continued with a full, three dimensional, numerical algorithm written in FORTRAN code. This was compared to a full geometry, ray trace program, BEAM 4, which optimizes the curvatures, based on purely optical considerations.

Founded on numerical results, the characteristics of a faceted concentrator were construed. The numerical methodologies themselves were evaluated and categorized. As a result, the three-dimensional FORTRAN code was the method chosen to construct the mirrors, due to its overall accuracy and superior results to the ray trace program. This information is being used to fabricate and subsequently, laser map the actual mirror surfaces.

Evaluation of concentrator mirrors, thermal applications and scaling the results of the 10 foot diameter mirror to a much larger concentrator, were studied. Evaluations, recommendations and pit falls regarding the structure, materials and facility design are presented.

TABLE OF CONTENTS

Section	Page
LIST OF FIGURES	IV
LIST OF TABLES.....	V
I. INTRODUCTION.....	1
II. SUMMARY.....	3
III. APPARATUS DESIGN AND FABRICATION.....	4
A. FACET FABRICATION.....	5
B. FRAME ASSEMBLY.....	7
C. HELIOSTAT.....	8
D. ACCOUTERMENT SYSTEMS.....	9
E. THRUST MEASUREMENTS.....	10
IV. NUMERICAL CALCULATIONS.....	10
A. TWO DIMENSIONAL ANALYSIS.....	11
B. THREE DIMENSIONAL ANALYSIS.....	14
1. <i>Surface Matching Algorithm</i>	14
2. <i>Ray Trace Analysis</i>	18
3. <i>Two Dimension Results in Three Dimension Reality</i>	20
V. FOLLOW-ON RESEARCH.....	20
VI. CONCLUSIONS AND RECOMMENDATIONS.....	21
REFERENCES.....	24
APPENDIX.....	25
FORTRAN CODE.....	26
FORTRAN INPUT.....	35
FORTRAN OUTPUT.....	36
BEAM 4 INPUT.....	37
BEAM 4 OUTPUT.....	38
APPARATUS COMPONENT PICTURES.....	41

LIST OF FIGURES

FIGURE 1: FACET LAYOUT FOR 10 FOOT MIRROR.....	2
FIGURE 2: UAH SOLAR LABORATORY.....	3
FIGURE 3: CURVE GEOMETRY.....	11
FIGURE 4: APPARATUS LAYOUT.....	12
FIGURE 5: TWO DIMENSIONAL SOLUTIONS.....	12
FIGURE 6: FACET ON PARABOLOID.....	15
FIGURE 7: SPHERICAL OVERLAY OF FACET.....	16
FIGURE 8: COMPARED RADIAL SOLUTIONS.....	17
FIGURE 9: TILT AND PITCH ANGLES.....	19
FIGURE 10: BEAM 4 LAYOUT.....	38
FIGURE 11: FOCAL IMAGE.....	38
FIGURE 12: GROUP 3 FOCAL POINT IMAGE.....	39
FIGURE 13: GROUP 3 FOCAL POINT 3-D INTENSITY.....	39
FIGURE 14: GROUP 14 FOCAL POINT IMAGE.....	40
FIGURE 15: GROUP 14 FOCAL POINT 3-D INTENSITY.....	40
FIGURE 16: FACET CASTINGS.....	41
FIGURE 17: LASER MAPPING EQUIPMENT.....	41
FIGURE 18: MIRROR FRAME AND SMALL MIRROR.....	42
FIGURE 19: HELIOSTAT FRAME.....	42
FIGURE 20: FACET RIB DESIGN.....	43

LIST OF TABLES

TABLE 1: SOLAR ANGLES AND HOURS OF OPERATION	8
TABLE 2: TWO DIMENSIONAL RESULTS	13
TABLE 3: TWO DIMENSIONAL OFFSET RESULTS	13
TABLE 4: THREE DIMENSION CODE RESULTS	17
TABLE 5: 2-D FITS IN BEAM 4 CODE	20

I. Introduction

The sun provides a constant energy source which can be harnessed for space and ground based applications. Thus, unlike other space propulsion or power systems that need to contain their own energy source, a solar engine affords a distinct advantage. The sun furnishes relatively diffuse electromagnetic radiation that requires concentration and then efficient transfer to a working fluid. Subsequently, at these high temperatures and pressures, a confined working fluid provides a convenient source for mechanical energy. This can be accelerated as rocket propellant to produce thrust or used in a heat engine. Theoretically, solar thermal rocket engines offer specific impulses of 800 to 1500 seconds. Other uses of concentrated solar energy include material processing, hazardous waste disposal and solar furnaces.

Solar thermal energy is ideally captured and concentrated with a parabolic conical mirror. Orbital hardware is perceived to be an inflatable, thin-film structure to minimize the system mass and upper stage launch volume. These fragile, one time use, concentrators are not practical for long-term, ground based mirrors, which are utilized as test rigs for fundamental hydrogen gas and solar absorber experimentation. The smoothly varying surface of a conical mirror is difficult to manufacture as a single, large structure. Fabrication costs grow exponentially for a continuous, solid concentrator, as its size increases beyond two meters (corresponding to typical, commercially available, lathes). Therefore, faceted mirrors are considered the most feasible solution.

In an effort to evaluate the techniques and optical qualities of a large, NASA, solar concentrator (nearly eighteen feet in diameter), a small faceted mirror is being constructed at the University of Alabama in Huntsville (UAH). This smaller mirror (Figure 1.) is a ten foot diameter concentrator with a focal point of nine feet (rim angle of 29 degrees). After its design, fabrication and optical evaluation, the mirror will be used in high temperature research, for the solar thermal rocket. The concentration ratio is over 8000 to 1 and maximum power is expected at 5,000 watts. The nominal one inch spot size is anticipated to produce temperatures near 3000 degree Kelvin.

Designing and producing small "pieces" of a continuous paraboloid is difficult, due to the continually varying geometry of each unique facet. The spherical approximation to the parabolic curve has been utilized to provide a symmetric geometry, which is more easily mass produced.¹ Unfortunately, this does induce optical aberrations and a larger focal point, spot size, as the parabolic curve can only be precisely matched at one point. All other points, along the spherical curve, will increasingly diverge and increase the optical error, the farther they are from the coincidence point.

This study began from the most basic assumptions and conducted research with two and three dimensional models. Although similar to imaging optics (e.g. telescope and microscope), a solar thermal concentrator is concerned with concentrating all the electromagnetic energy and not with maintaining its particular orientation (i.e. image). The interest here is to obtain the smallest, spot size and highest intensity possible, at the lowest cost, while being easily scaled for extremely large concentrators.

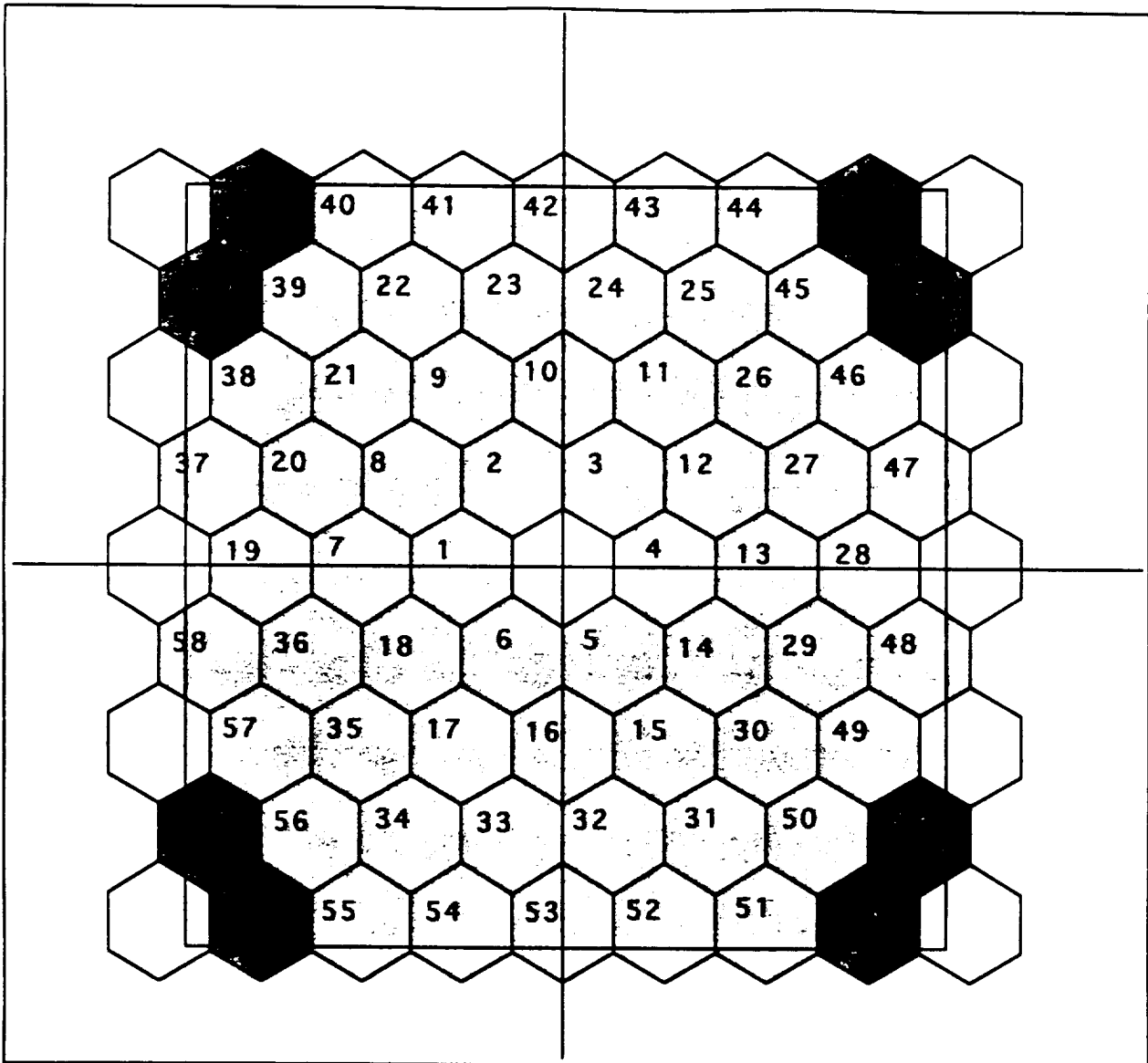


FIGURE 1: FACET LAYOUT FOR 10 FOOT MIRROR

Three different methods of determining the optimum spherical curvature were investigated. This computer analysis quantifies the error associated with the spherical approximation. The results reveal the spherical geometry that best fits the selected parabolic concentrating mirror for each individual facet. In the most advanced algorithm developed, the full three dimensional surface is accounted for. Thus, the error induced by the symmetry of the facet, superimposed upon the asymmetric paraboloid, is not neglected, as it is in the two dimensional approach.

The data from the analysis conducted will be utilized in machining an aluminum concentrator, constructed of eighteen inch diameter, hexagonal facets. The evaluation of the entire mirror, as well as the individual facets, will be compared to the numerical performance predicted in this study. The mirror design also incorporates some unique manufacturing approaches and cost effective methods in its fabrication. This rigid

collector is to be compared to a thin-film, membrane mirror, mounted on a machined ring. These two systems are being assessed, in the UAH Propulsion Research Center's newly completed solar thermal laboratory (Figure 2).



FIGURE 2: UAH SOLAR LABORATORY

Other mirror types (i.e. inflatable and Fresnel) have also been proposed for use as solar thermal concentrators.² These, too, are expected to be examined in the same manner and compared against the faceted mirror's performance. The ultimate objective is to test and evaluate a small, windowless absorber, for a solar thermal upper stage.³ However, the fixed solar collector has many other uses in material research, fluid dynamics and heat transfer experimentation.

II. Summary

This study centered on the faceted mirror concentrator for research and laboratory use. The mirror is comprised of solid aluminum, hexagonal pieces and is generally considered inappropriate for direct space applications. The curvature of each facet was calculated by several methods. The most precise was a full three-dimensional FORTRAN program.

Casting the facet was considered to be the most economical fabrication method. The cast aluminum alloy selected was A535. Each facet is individually focused using two adjusting rods and a single, center ball joint, mount. The frame for the concentrator was kept flat over much of the surface with the edges bent 20 degrees

toward the focal point. For simplicity, axial positions are adjusted over a long 9" threaded rod.

The solar energy is directed into the laboratory by a heliostat. This sun tracking, flat mirror affords a fixed source of solar energy to a protected concentrator and test chamber, within the facility. Furthermore, it is easier to rotate the relatively small heliostat, than the entire concentrator with its diagnostics and vacuum chamber. The main detriment to this approach was the losses involved with an extra mirror optic. The flat mirror selected was a lightweight, fabric backed, glass mirror attached to an aluminum frame.

Solar thermal testing was to be conducted in a vacuum chamber to simulate the space environment. An 18" diameter tank with a quartz window is used for this purpose. Pressure, temperature and flow measurements were set up to conduct high temperature tests with various gasses, including hydrogen (the most likely propellant for a solar thermal upper stage). An infrared sensor was chosen to observe the focal point energy from the faceted mirror center. The gas flow meter was determined to be the most critical measurement device for the solar thruster experiments. A highly accurate mass flow controller was installed to handle flows up to 100 Standard Liters per Minute (SLM). Direct thrust measurements were investigated late in the contract. A scheme for assembling and calibrating the low forces expected from a solar rocket was devised.

Other applications, of highly concentrated solar energy, were examined. Reutilization of the Space Shuttle's external fuel tank, as stock material, was considered feasible using an orbiting solar furnace. However, no direct tests on the aluminum tank shell were conducted.

To evaluate the performance of the faceted mirror, as well as, other candidate mirrors, a laser mapping apparatus was constructed. Two alternate methods were also investigated for concentrator characterization. Actual mirror facet evaluations were not conducted due to the unexpected, nonavailability of NASA polishing and fabrication support of the finish mirror surfaces.

III. Apparatus Design and Fabrication

After review of Marshall Space Flight Center's (MSFC) preliminary plans for an 18 foot solar concentrator (Hot Hydrogen Test Bed planned for construction near building 4583), a preliminary layout of a small structural frame and the mirror shapes were outlined. An eight foot version was concluded as sufficient to demonstrate the applicable mirror properties. The test mirror's only difference from the large scale version was that only the center facet was deleted, instead of the inner seven facets for the large collector. Later it was recommended to expand the simple eight foot diameter concentrator to a ten foot mirror (by adding a fourth ring), so the total energy of the concentrator could be used for material tests, as well as, low thrust (i.e. 1/4 lb.) solar rocket evaluations.

The entire test system was broken down into four major areas. The concentrator frame, the mirror facets, the heliostat and the supporting test systems. These test

systems included the vacuum chamber and pumps, thrust stand (for the rocket tests), gas supply system and data acquisition components.

A. Facet Fabrication

Originally, the design for the multi-faceted mirror was to be one half inch 6061 T6 aluminum plate, polished on a diamond lathe, turning machine. A center ball joint would support the full weight of the mirror with two adjustment screws (placed at the 3 and 6 o'clock positions on the back edge of the facet) to "fine tune" the final mirror facet placement. The facets were to be formed as a spherical approximation to a perfect parabolic concentrator. Each facet mirror shape was calculated so that the intersection of the parabolic curve and the spherical radius occurred at the center of the facet. Therefore, within the accuracy of the machining and the final adjustment of the mirror center, the ideal focal point was expected to only spread due to the maximum slope deviation at the edge of the facet. The actual solar collection tests would have the additional deviation of the solar angle (approximately 1/2 degree angle) which will tend to increase the focal spot size. A nine foot focal length was set for the concentrator, to keep the rim angle less than thirty degrees. Two adapter plates required to match up the facet bolts and the lathe mandrel mounting plate, were made for the MSFC diamond lathe machine.

The first facets were constructed from one sheet of 6061-T6 aluminum (provided from MSFC existing stock). As the metal was being cut and mounting holes machined, a warp of several thousandths of an inch was noticed (probably due to the poor storage of the metal outside). For most uses, this would be negligible. However, for the high quality mirror shape required for the program, it was suspected that it would cause considerable surface error.

After one facet was rough cut for the spherical surface, the plate experienced internal stress relief. This warped the plate so much that the curvature was very unsatisfactory for a concentrator. The correction proposed, was that the plates would be heat treated. The first three facets were used to determine the best conditions and time to treat (i.e., before and/or after the rough surface cut).

The initial tempering results (three hours at slightly below the material melting temperature) were unsatisfactory. In addition, the depth to be cut in the center of the facet was nearly the 1/16 inch available depth in the plate. One facet center actually broke through the center, where the backside had been drilled and tapped for a mounting bracket. Increasing the thickness from 1/2 to 3/4 inch thick aluminum plate was considered to be barely adequate to prevent the warping and mounting difficulties. Realistically, the plate needed to be 7/8 to one inch thick. It would still require a two step heat treatment (before and after the rough cut machining was done). Consequently, this would impact the entire frame size and the adjustment design to handle the extra weight. Due to the cost increase, as well as, the extra handling time and effort required by the MSFC machinists, other viable methods were considered.

The most promising alternate approach investigated, was casting the facets (Figure 16. on page 41 in the Appendix). This allowed a ribbing structure to be easily incorporated into the back, making the facet more rigid but lightweight. The casting approach also eliminated the time and expense of cutting the hexagonal shapes from

flat stock. Furthermore, the casting afforded the opportunity to cast a rough dish shape into the front surface. This had the potential of eliminating (or at least greatly reducing) the need of any rough cutting on the diamond turning lathe.

After some searching around the country for a suitable supplier of aluminum castings, C&B Foundry, a local metal casting company, was selected to do the work. Although there were several foundries who specialized in the casting of optical parts, the cost of 36 to 60 facets was excessive (\$100 to \$500 per facet). The key cost difference was in the specific aluminum alloy used for the part.

The material specified by C& B Foundry was A535 aluminum alloy. This is the best material available considering the total product cost. A201 aluminum alloy provides slightly better optical qualities and was offered by two of the most expensive suppliers contacted. The properties of the A535 alloy was very satisfactory for the solar concentrator. The castor's production method was good, based on the small samples taken from a typical product run. Special care was given to limit the porosity within the facet during each production run. Samples machined easily (the material was somewhat softer than the 6061-T6 aluminum plate) and produced an excellent surface finish.

The first six facets picked up from the casting foundry appeared satisfactory in size, design shape and metal quality. There was a slight dip in the center mounting area (on the back) and some of the pieces did not have a pronounced curve shape to the front face. This did not cause significant difficulty to the machining or construction although the casting mold was modified to increase the front dish shape.

Two mirror facets were heat treated at 700 degrees Fahrenheit at MSFC. They were satisfactory but slightly "softened" in strength. Further heat treatments would be conducted at slightly lower temperatures. For optimal mirror results, the rough cut was made before the heat treatment process, on those facets that were too flat.

The facets were originally conceived to be mounted to the lathe using the same tapped holes on the back of the mirrors. Several conflicts arose with the heat treat process, using heilcoil inserts in the casting, mounting position layout and difficulty in lath mounting. Through holes were used to secure the facet on the lathe with counter sink holes in the face to allow simple attachment to the machine. These holes were not used for any other purpose and left small openings in the finished mirror surface. Heilcoil inserts were used for adjuster mounting but not installed until the entire facet polishing was finished.

During the polishing of the first facet that was cast, it was noted that a harmonic vibrational mode was causing small rings in the polished surface beyond the radius of the three bolts. Even at very low rotational speeds, the problem was evident. This forced several modifications of the cast, used to make the mirror facets. The support ribbing was increased in size and extra ribs cast on the perimeter (Figure 20. Appendix page 43). These stout castings are much less susceptible to the vibration problem. It was hoped they would have a more pronounced curvature and preclude (or at least reduce) the rough cutting process on the diamond lathe. However, premachining was added to the fabrication procedure to ensure the best finish and impose the least amount of time on the MSFC lathe. (Machine availability became the critical path item for the entire program).

A standard machine lathe was modified, at the UAH Student Machine Shop, to cut the rough curve of an eighteen foot diameter sphere into the facet surface. This and all the machining for mounting hardware was done within the Propulsion Research Center. This allowed the program funding to be stretched, enabling a full 66 faceted mirror to be made. Unfortunately, the lack of machine access at both MSFC and the University (for several months at a time) and the foundry delays (caused by unacceptable forecasts of humidity and air temperature during the processing time) blocked completion of the mirror before the contract end date. The work will continue as a university research program.

Although the concentrator is housed in an enclosed environment (except when the laboratory bay doors are open during operation) protection of the highly polished mirror surface is of concern. The facets were expected to be coated to protect their fine surface. Both a clear coat and a highly reflective, protective, coating were investigated. Nickel or clear anodize seems to be the most promising for use as coatings. Because limited program time and funding, test sample coatings were planned but were not made. Surprisingly, an unprotected facet showed very little surface degradation over a six month period inside the lab environment.

B. Frame Assembly

The concentrator frame requirement was to hold each facet rigidly in place, to form a smooth parabolic shape over the whole concentrator. The facet placement was critical, so individual adjustments were prudent for each facet. The frame load carrying members could be crudely shaped to form a dish shape. For the small ten foot diameter concentrator, the inner rings of facets were nearly flat and the curvature was taken into account by the position adjusting mechanism. Only the outer ends were bent at a 20 degree angle toward the focal point. The structural requirements of the small mirror allowed some simplicity and cost savings to be in the design. Unlike a larger concentrator, which starts at the third facet ring, the flat design here was feasible.

Two mounting arrangements were investigated for use on the facets. The center ball joint support relied on a single main support to hold the facet weight. Two small adjustment rods were added to the facet at 90 degrees apart. The Z-coordinate adjustment was made with the center support and the tilt and/or pitch angles were made with the smaller threaded rods.

The alternate design had three identical adjustment arms. Both ends of the arm had a friction type ball joint and the three are spaced 120 degrees apart. Each supported part of the facet weight and its turnbuckle was used as the adjustment to angle the mirror. The advantage with this was the commonality of the parts being more economical and the single, small end plate needed to be attached to the frame. However, the support of each facet was weak, relying on friction type ball joints for a nearly horizontal brace. The eventual cost and availability of these adjusters made them impractical for the small concentrator. Moreover, the direct center mounting design had corresponding angle adjustments, which were directly generated by the computer codes (i.e. tilt and pitch values).

The final effort produced 120 quarter-inch ball joint adjusters and 60 half inch center support studs. An equal amount of mounting plates (with threaded centers) were fabricated at the PRC and mounted on the frame. The concentrator support frame required almost 1000 mounting holes and nearly 400 fasteners (pictured in the background, Figure 18. on page 42 in the Appendix). In addition, the frame members were heated and bent to form the dish shape curvature of the concentrator. The fine threaded rods (28 threads per inch) adjust the facet to within a degree of accuracy.

C. Heliostat

The ten foot concentrator required a larger heliostat surface to direct the sunlight into the bay door. It was calculated that a 12x14 square foot surface permitted solar tracking for at least 3 hours each day (year round). Table 1 shows the estimated operational times and angles for the system. Originally the building was to be a full two feet higher than the heliostat to accommodate the extra mirror length, in the full vertical position. This was not accomplished and the center support pipe must be manually raised up sixteen inches to permit near vertical positions. This operation would be impractical on a larger system. A hydraulic or geared motor was considered for this design, but dropped to keep within budget constraints.

TABLE 1: SOLAR ANGLES AND HOURS OF OPERATION

	SUMMER			WINTER		
	Start	Peak	End	Start	Peak	End
Hours	10:30	12:00	2:30	10:30	12:00	1:30
Altitude	64	79	54	25	32	25
Azimuth	43.5	0	72.5	21.5	0	21.5

The tracking mechanism is a two axis platform. The base component was from an abandoned heliostat, at the Alabama Solar Energy Center. The housing was rebuilt and significantly reinforced to handle the large 750 pound mirror. This included a new motor and larger main bearing. A large aluminum frame was constructed (Figure 19. page 42 in the Appendix) and the flat mirrors were offset by set screws. These permitted the adjustment to the mirror panels to correct any slight irregularities in the glass or the aluminum frame.

A commercially available, plate mirror (3 millimeters thick) was selected for the heliostat. It is lighter than standard plate glass and has a fabric laminated back, which gives it strength and protects the reflective silvering from the elements. It is normally utilized for safety purposes to keep the glass from shattering apart. When an extra layer of sealant was added, it became an excellent weather proofing system for the mirror silvering. The thin mirror provides some flexibility for the adjustment screws and withstands minor bumps or mishandling. The surface reflectivity was equal to the best commercially available glass mirror (about 90 percent) and the surface finish quality was acceptable. A rigid foam pad was used to cover the glass when not in use. Plans

for further protection (i.e a containment box) and support during high wind conditions were suggested. However, they were not implemented, since the total cost of this test equipment did not warrant the high expense of an enclosure. The heliostat was estimated to withstand sixty mile per hour winds.

D. Accouterment Systems

Several periphery systems were needed to complete a ground test facility for high temperature, solar experiments. The spaced based applications and the solar material processing furnace had a vacuum requirement for testing. Isolation from convective heat transfer effects was necessary in other research areas as well. A gas supply system is required in the propulsion and power investigations. Temperature, pressure and flow conditions needed to be monitored by a high temperature (near 3000 degree Kelvin) data acquisition system.

A small vacuum chamber was sized, to obscure the center mirror facet. This provided a maximum test width of 16 inches. The chamber front face and side walls were double walled to provide a cooling jacket. A six inch quartz glass window is used, in the front, for admittance of the solar energy. Even for the small apparatus assembled here, the calculated minimum clear view was 5.6 inches in diameter. A six inch glass window was also placed on the side for visual observation during testing. The tank was supported from a frame above the ten foot mirror height. Only a 1/2 inch wide by five feet long section obscured the mirror for supports, piping and diagnostic hardware. The vacuum lines were six 1/2 inch pipes, lined up behind one another, in a manifold arrangement. Twin vacuum pumps (30 CFM capacity each) were set up on the roof, directly over the test chamber. For the full operation of a 1/4 pound rocket engine, these pumps alone were unable to maintain an acceptable vacuum (i.e. 1 psi or less). An additional 100 CFM capacity is estimated to be needed and could be connected by extending a four inch manifold and auxiliary tank above the test chamber.

The pressurized supply system utilized bottled nitrogen and hydrogen gas, but a variety of other gases or additional seed gases can be accommodated in future tests. Cryogenic hydrogen was determined to be too hazardous for the university laboratory site and the added expense was greater than the perceived research advantage gained. The flowmeter and controller was critical to the rocket propulsion test uncertainty analysis. Gas temperature and pressure transducers were installed to obtain the supply gas condition. The bottles and supply system were housed in a small concrete block shed, outside the laboratory. An automatic nitrogen purge system was included for safety when running hydrogen, as well as, an explosion proof fan for ventilation.

A drop-screen was fabricated to provide a quick method of cutting off the solar energy input to the concentrator. This electric solenoid activated device was for emergency shutdowns. However, the actual mechanism only proved to work marginally. Defocusing the heliostat directly was almost as fast an operation.

The data acquisition system required mostly standard equipment. The computer and input boards were commercially available, as were the sensors and flow controller. The thermocouples had to be extreme high temperature capable (above

4000 degree). Tungsten/Rhenium was available and provided the proper temperature range. The most unique sensor was an infrared thermocouple which could provide an average temperature of the absorber surface or the furnace material at the hottest spot (i.e. the concentrator impingement spot). The sensor's long distance optics (five foot focal distance) were barely adequate to keep the sensor head from blocking any of the concentrated solar energy, as it was held out on a boom from the center of the concentrator.

E. Thrust Measurements

The design for a low thrust measurement apparatus was made in anticipation of solar thermal rocket tests. The facility was limited to a maximum total vacuum thrust of 1/4 pound. Two identical load cell (strain gauges) are rigidly attached to the vacuum chamber wall. They are set against a machined ring, which is suspended from light wire fibers (six individual strings, spaced evenly around the ring outer diameter). Alternate arrangements include an extremely friction free bearing (ball bearing, knife edge, rail, etc.) or overhanging the ring on the load cell itself. The thruster to be tested is held, fixed by mounting screws, in the center of the ring.

Calibration correlations are to be made in two ways to limit the uncertainty of the final measured force. The entire system is set up without connecting the thermocouple wiring and the propellant supply line. A highly accurate load cell gauge is applied to the front face of the absorber entrance and several measurements are to be taken over a range of operating temperatures (300 to 2300 Kelvin). The same procedure is used for a spring strain gauge but it is attach to the nozzle and pulling instead of pushing the thruster. These two measurements will provide a good estimate of the effect of the support wires on the measured thrust. The results can be plotted to indicate the trend of the temperature gradient on the system. However, no effect is predicted, due to the relatively small heat flux and the well insulated/isolated rocket engine.

The same procedure is planned with the piping and wiring connected to the absorber. The propellant supply line is anticipated to have a noticeable impacted on the measured thrust. Again calibrations can be drawn from such a data series and an estimate of the uncertainty obtained. The final values of an engine test can be compared to the calculated thrust from the known propellant flow rate, bulk gas temperature difference or the estimated heat flux to the absorber, nozzle geometry and vacuum conditions.

IV. Numerical Calculations

The critical effort in the research was the determination of the ideal spherical curvature for the facet. Each facet was considered separately. The numerical analysis progressed from simple to the most complex approach. Finally, the simple two dimensional results were evaluated using the full three dimensional programs.

A. Two Dimensional Analysis

The two dimensional approach simply overlays the parabolic line with a circular one. The first curve fit case (Centered Circle) fixes the curves' intersections at the origin. The circle's arc is fit symmetrically on the parabola, tangent to its center and with the circle's radius along the Z axis (left side of Figure 3.). This is the simplest geometry and easiest calculation to make.

The calculation optimized this curve fit, by iteration (forward differencing) of the circle radius and comparing the Y-coordinate differences between the curves using 183 grid points. The error in the table is based upon the cumulative linear distance, between the two curves (parabola and circle), at each grid location. Since the

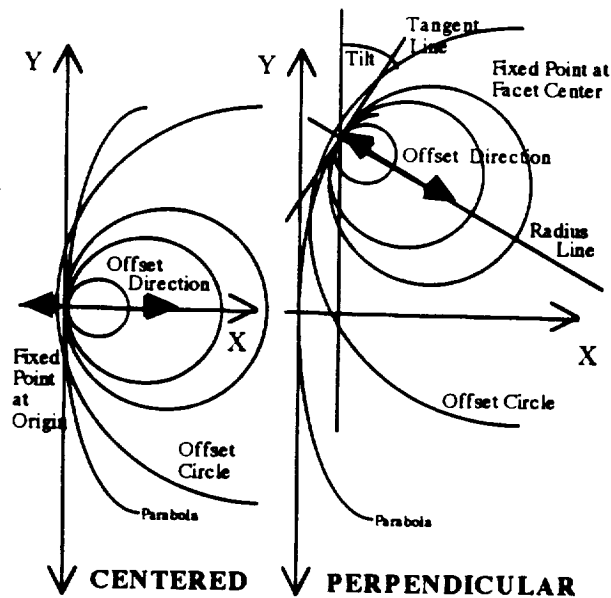


FIGURE 3: CURVE GEOMETRY

cumulative error is essentially arbitrary (the more grid points, the greater the nominal error value becomes), the values were normalized by dividing by the total number of points.

The center mirror facet (Mirror #0) was evaluated as a reference point. However, this mirror has been eliminated from the actual facet concentrator, since it was hidden with a shadow cast by the vacuum test chamber. The chamber was judiciously sized to obscure only the center facet, as illustrated in Figure 4. The resulting radius of curvature (2-D solution) is 18.005 feet. The two curves matched very closely over the rather short facet length of 18.25 inches. The other facet curves were approximated with the same analysis. The sixty six, individual facets, which comprise the concentrator, were divided into groups. All facets in a group are optically identical, due to the symmetry of the four coordinate axis quadrants.

The farther the facet is from the origin, the greater the curvature deviates. The results for the outer facets were very poor as one might imagine. Results of the "Centered" geometry are listed in Table 2. for all 14 groups, along with their average

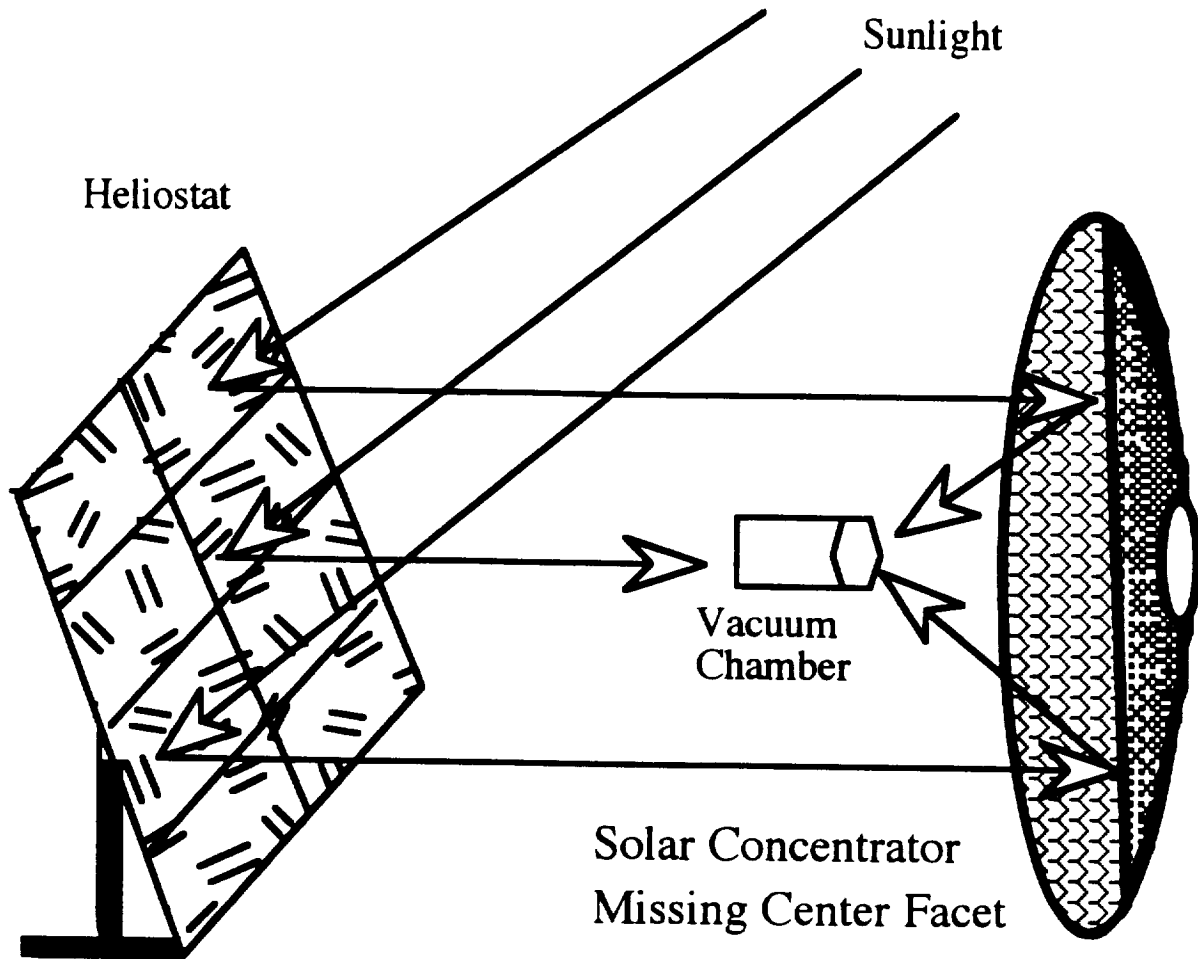


FIGURE 4: APPARATUS LAYOUT

error per grid point, in inches. The Tilt column is the angle of the tangent line to the Y axis.

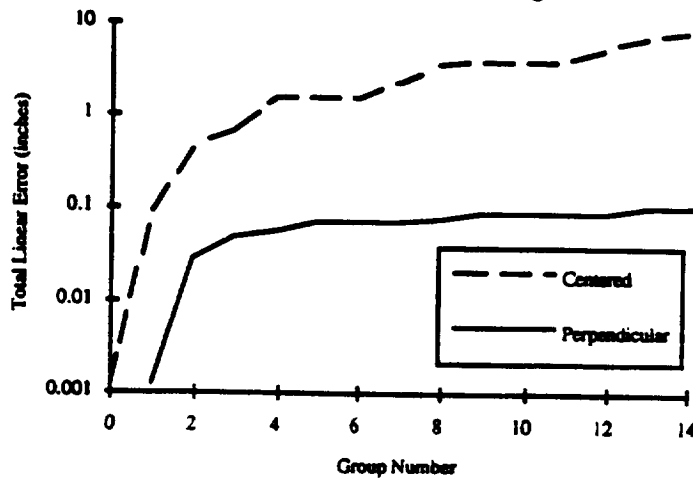


FIGURE 5: TWO DIMENSIONAL SOLUTIONS

TABLE 2: TWO DIMENSIONAL RESULTS

Group	Facet Center	Centered			Perpendicular			
		Radius (inches)	Total Error	Error/Pt (inches)	Radius (inches)	Tilt (degrees)	Total Error	Error/Pt (inches)
0	0.0000	216.061	0.00118	6.44E-06	216.061	0.000	0.00118	6.44E-06
1	15.8050	216.462	0.08562	4.68E-04	217.639	4.185	0.02731	1.49E-04
2	27.3750	217.059	0.43287	2.37E-03	221.2	7.223	0.04686	2.56E-04
3	31.6099	217.353	0.66558	3.64E-03	223.114	8.326	0.05383	2.94E-04
4,5,6	41.8160	218.23	1.54225	8.43E-03	228.535	10.957	0.07008	3.83E-04
7	47.4149	218.812	2.25243	1.23E-02	232.156	12.381	0.07864	4.30E-04
8	54.7500	219.685	3.47917	1.90E-02	237.615	14.223	0.08940	4.88E-04
9,10,11	56.9856	219.969	3.92749	2.15E-02	239.427	14.779	0.09257	5.06E-04
12	63.2199	220.844	5.38224	2.94E-02	244.917	16.314	0.10114	5.53E-04
13	68.8922	221.715	6.99126	3.82E-02	250.45	17.690	0.10857	5.93E-04
14	72.4274	222.287	8.14478	4.45E-02	254.173	18.537	0.11302	6.18E-04

The second approach is a more practical two dimensional analysis, since each facet is considered radially symmetric. The approximating circle is positioned with one curve point passing through the center of each facet. Using this axis-symmetric orientation, a practical mirror can be machined by a conventional lathe. Taking the derivative of the parabola, the circle radius is held perpendicular to the parabolic curve's tangent line, at the facet center (reference the left side of Figure 3). Optimization of the circle radius delivers reasonable results, with the two arcs nearly overlapping each other perfectly, especially over the short facet diameter distance (note Table 1. provides these statistics). Again, the total error is divided by the number of points to give an average error value. There is an order of magnitude reduction in line deviation (i.e. error) with this second technique. Using a log scale, Figure 5. graphically demonstrates this fact.

The above two analyses (Centered and Perpendicular) were further optimized by varying the intersection point(s) of the two curves. Instead of a designated central curve cross, the entire circle was displaced along the line, perpendicular to the parabola's tangent (Figure 3. illustrates this by the dotted line). The Centered Circle

TABLE 3: TWO DIMENSIONAL OFFSET RESULTS

Group	Facet Center	Circle Centered					Circle Perpendicular				
		Radius	Offset	Error	Error/Pt	% Change	Radius	Tilt	Offset	Error/Pt	% Change
0	0.00000	216.0730	0.000005	0.001021	5.58E-06	13.322	216.0729	0.0000	-5.44101E-06	5.44E-06	15.546
1	15.80496	216.6769	0.000775	0.048402	2.64E-04	43.472	217.6027	4.1849	6.2083E-07	1.49E-04	0.019
2	27.37500	217.8374	0.007000	0.145041	7.93E-04	66.494	221.1751	7.2229	3.59242E-09	2.56E-04	0.000
3	31.60993	218.4048	0.012313	0.193321	1.06E-03	70.954	223.1734	8.3257	-4.54698E-07	2.94E-04	0.004
4,5,6	41.81600	220.1150	0.037346	0.338211	1.85E-03	78.070	228.6464	10.9565	-1.89668E-06	3.83E-04	0.023
7	47.41489	221.2522	0.061467	0.434757	2.38E-03	80.698	232.3073	12.3808	-3.24185E-06	4.30E-04	0.034
8	54.75000	222.9485	0.108583	0.579614	3.17E-03	83.340	237.7835	14.2233	-4.26451E-06	4.88E-04	0.051
9,10,11	56.98561	223.5116	0.127168	0.627898	3.43E-03	84.013	239.6040	14.7792	-4.42247E-06	5.06E-04	0.056
12	63.21985	225.1881	0.191173	0.772774	4.22E-03	85.642	245.1605	16.3139	-6.43531E-06	5.52E-04	0.070
13	68.89224	226.8342	0.266640	0.917644	5.01E-03	86.874	250.6874	17.6899	-7.05873E-06	5.93E-04	0.083
14	72.42744	227.9312	0.323960	1.014187	5.54E-03	87.548	254.4304	18.5369	-8.2705E-06	6.17E-04	0.091

case was greatly improved with offset adjustments, although it still had 10 times more error when compared to the Perpendicular case (see Table 2.). Surprisingly for the latter case, the optimized offset distance was less than one micron. With a correspondingly minute change in radial curvature, only a slight percent change in error was noted in most of the perpendicular groups.

B. Three Dimensional Analysis

Much effort was expended to account for the non-symmetrical character of the parabolic segment with a symmetrical facet. This led to the writing of a FORTRAN code to generate three dimensional surface geometries. The program is similar to the grid development of a finite difference, numerical scheme used for fluid or heat transfer algorithms. To check the output, a comparison was made with BEAM 4, a commercially available program. This software uses light ray tracing to "illuminate" an optical system. It also has an optimization algorithm to determine the best curvature for the mirror and the positioning of each facet. A Monte Carlo simulation, which disburses random rays across the concentrator, is supplied with the program to evaluate the focal point, energy flux.⁴ Both the FORTRAN and BEAM 4 codes include full, three dimensional, geometrical considerations. The results of the two dimensional analysis were used as input to the two codes above and evaluated.

1. Surface Matching Algorithm

To fully account for the three dimensional geometry of the hexagonal facet shapes, a computer code was written to evaluate the radius of curvature, orientation and deviation from the ideal concentrator. The result was a 500 line FORTRAN program that performed a surface mapping optimization for each spherical facet and compared it to the true parabolic surface it was representing.

Figure 6. shows a typical facet oriented in three dimensional spatial coordinates, as it lies on the parabolic curve. One mirror facet at a time is calculated to fit the parabolic curve. Each facet is rotated by means of a series of coordinate transformations. Not only does this properly place the facet center on the paraboloid, but it aligns the facet's centerline plane with the tangents (i.e. in the X-Z and Y-Z planes) to the parabolic surface. The program calculates a sphere, positioned along the paraboloid's normal line and passing through the midpoint of the facet plate (see Figure 7. and similar geometry of the Perpendicular case, shown in Figure 3.). Varying the radius generates a series of spheres, each of which is evaluated over a fine grid and compared to the ideal, parabolic position. The total error, over all the spatial coordinates, is summed and plotted. As a fine tuning to the curvature matching, the depth that the sphere penetrates the parabolic surface is varied independently of the spherical radius. Generated plot and data outputs from the resulting cases are evaluated, thus revealing the best spherical approximation to the paraboloid concentrator, for individually faceted mirrors (representative of Figure 7.). The program's methodology is shown in the following subroutines:

- Define Facet Grid
- Rectangle to Polar Coordinate Transformation for Facet Grid
- Facet Translation
- Calculate Facet's Paraboloid Surface Coordinates
- Radius "Do Loop"
 - Determine Sphere's Center Coordinates
 - Calculate Spherical Coordinates for Facet
 - Calculate Root Mean Square (RMS) Error
 - Save Best Case
 - Shift "Do Loop"
 - * New Sphere Center Coordinates
 - * Calculate Sphere Coordinates for Facet
 - * Determine RMS Error
 - * Save Best Curve
 - * Calculate New Shift Point
 - Calculate New Radius
- Graphical/Numeric Output

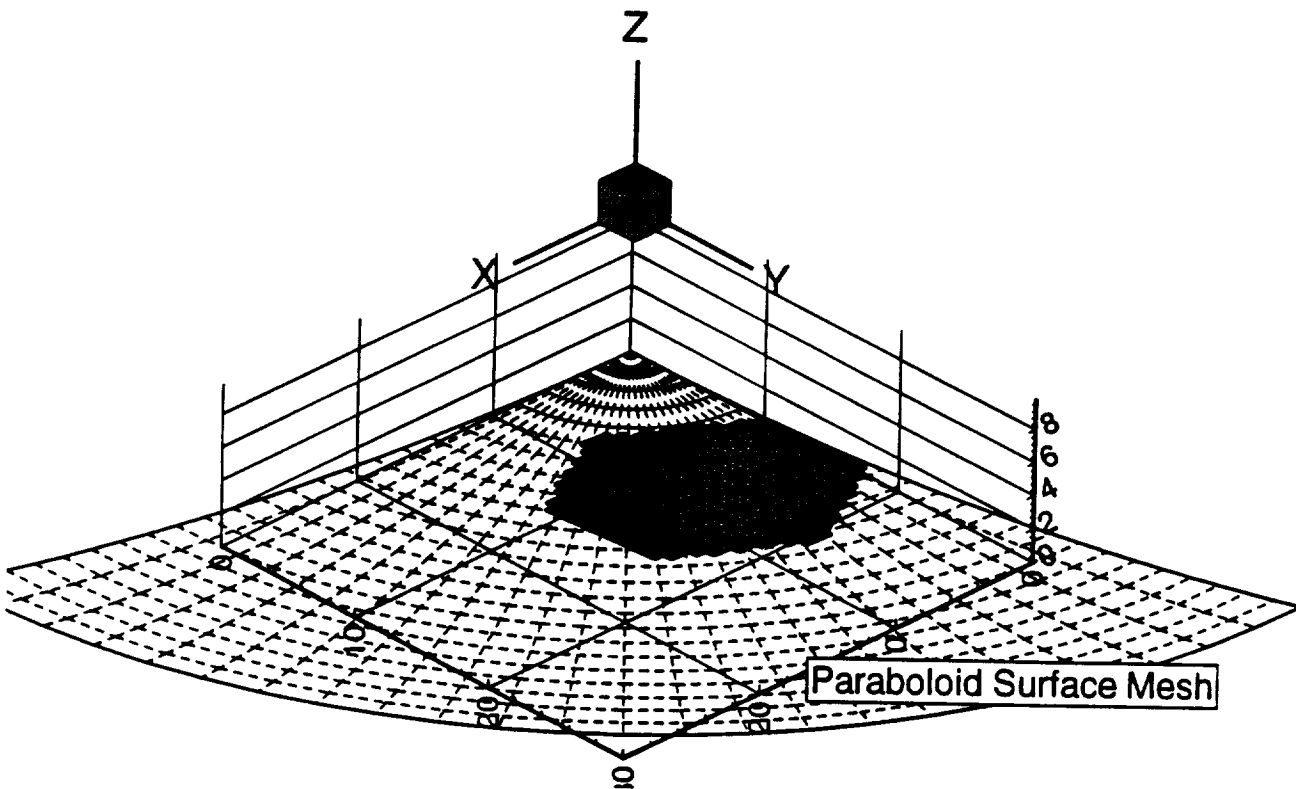


FIGURE 6: FACET ON PARABOLOID

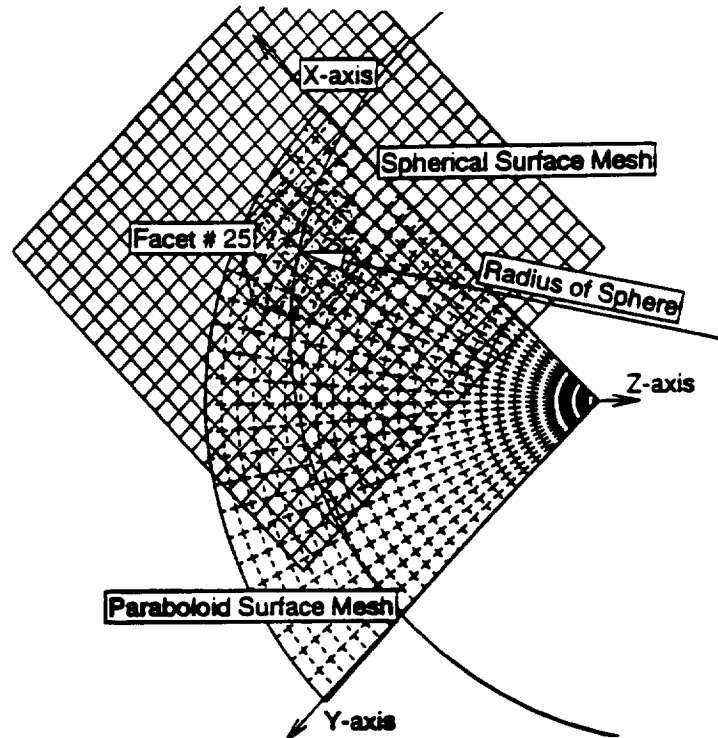


FIGURE 7: SPHERICAL OVERLAY OF FACET

The parabolic and spherical coordinates were determined from the solution of their rectangular equations:

$$z = \frac{(x^2 + y^2)}{4f}$$

$$r^2 = (x - h)^2 + (y - l)^2 + (z - k)^2$$

and the symmetric equation for a line (i.e. facet grid):

$$\frac{(x - x_1)}{A} = \frac{(Y - Y_1)}{B} = \frac{(z - z_1)}{C}$$

where the symmetric equation constants A, B and C are based on the facet grid points (X_1, Y_1, Z_1) and (X_2, Y_2, Z_2) .

The solution is straight forward and with careful code setup, was run on a 486/66 PC (for a 30x30 grid). Errors were noticed when very tight curve fits were attempted. Several steps were added to prevent round off errors from causing code termination, by overflow type code violations. When the code was used on a Cray XMP supercomputer, the double precision calculation had no problems and produced excellent results.

The grid was varied from a 15 x 15 to a 150 x 150 mesh. Below a 60 x 60 spacing, the code results did not converge consistently on an answer (although it was close in all runs). Above this, it was very consistent and no difference was seen among the cases. A 75 x 75 spacing was chosen as a good compromise between confident convergence and expending excess CPU time, while evaluating all 14 facet groups.

The cases were conducted in two successive runs. The first varied over a broad range of spherical radii and produced a narrowed radius bracket. The second program execution optimized the radius to within a thousandth of an inch. Radius

TABLE 4: THREE DIMENSION CODE RESULTS

GROUP	FACET NUMBERS	CENTER COORDINATE			BEAM 4				FORTRAN			
		X	Y	Z	RADIUS (Inches)	PITCH (Degree)	TILT (Degree)	RMS Deviation	RADIUS (Inches)	PITCH (Degree)	TILT (Degree)	RMS Deviation
0	0	0.0000	0.0000	0.0000	214.5539	0	0	0.01429				
1	1 2 3 4 5 6	7.9025	13.6875	0.5782	215.7109	2.0905	3.6249	0.01446	217.21	2.0953	3.6259	0.00037
2	8 10 12 14 16 18	0.0000	27.3750	1.7347	218.0629	0	7.2209	0.01484	219.483	0	7.2229	0.00059
3	7 9 11 13 15 17	15.8050	27.3750	2.3129	219.2582	4.1507	7.2209	0.01505	220.646	4.1849	7.2229	0.00178
4	20 27 29 36	39.5124	13.6875	4.0476	223.0069	10.3432	3.6249	0.01579	223.971	10.366	3.6259	0.00457
5	21 26 30 35	31.6099	27.3750	4.0476	223.0069	8.2583	7.2209	0.01579	224.125	8.3257	7.2229	0.00583
6	23 24 32 33	7.9025	41.0625	4.0476	223.0069	2.0579	10.7608	0.01579	224.028	2.0953	10.764	0.00147
7	19 22 25 28 31 34	23.7074	41.0625	5.2041	225.5639	6.1525	10.7607	0.01635	226.341	6.2635	10.764	0.00513
8	38 42 46 49 53 57	47.4149	27.3750	6.9388	229.5772	12.2822	7.2209	0.01729	229.892	12.381	7.2229	0.01244
9	37 47 48 58	55.3174	13.6875	7.5170	230.9469	14.3332	3.6248	0.01762	231.097	14.365	3.6259	0.00858
10	39 45 50 56	39.5124	41.0625	7.5170	230.9469	10.1851	10.7607	0.01762	230.947	10.366	10.764	0.01295
11	41 43 52 54	15.8050	54.7500	7.5170	230.9469	4.056	14.2159	0.05196	230.81	4.1849	14.223	0.00373
12	40 44 51 55	31.6099	54.7500	9.2517	235.1558	8.0718	14.2195	0.01870	234.251	8.3257	14.223	0.01115
13	59 62 63 66	55.3174	41.0625	10.9864	239.521	14.1184	10.7607	0.01985	237.807	14.365	10.764	0.02434
14	60 61 64 65	47.4149	54.7500	12.1429	242.5222	12.0094	14.2195	0.02067	239.952	12.381	14.223	0.02365

values for each group are indicated in Table 4., under the FORTRAN heading. Figure 8. shows the radius results of each of the "non-offset" cases.

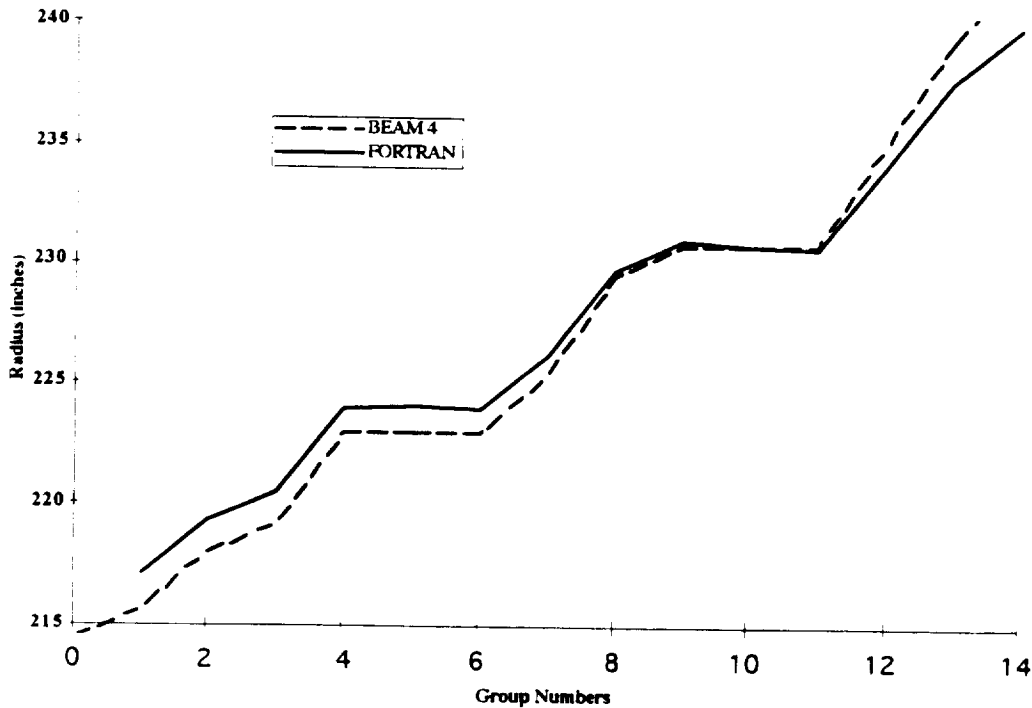


FIGURE 8: COMPARED RADIAL SOLUTIONS

As first seen in the two dimensional analysis, the spherical offset continued to be extremely small. The high precision calculations could optimize on a radius so close to the paraboloid (over the facet size), that the offset was nearly negligible. Most values were on the order of 1×10^{-6} inches, well beyond the calculation's significant digits. Since this calculation increased the run times exponentially, half of the facet cases were completed without any offset optimization. This was valid, since the offset correction is actually applied to the facet's mounting position. The concentrator frame and related alignment apparatus has a crude accuracy of about one hundredth of an inch, at the very best. Therefore, any misalignment would far exceed the potential accuracy gained using the offset radius.

2. Ray Trace Analysis

The complementary numerical analysis, to the three-dimensional surface fitting algorithm previously discussed, is the optical ray tracing code, BEAM 4. A typical, optical, input file (Appendix: BEAM 4 Input) generates the facet mirror by overlaying three rectangular irises in front of a circular, reflective optic. The program optimizes the pitch, tilt and radius of curvature, for the mirror. It also outputs the Root-Mean-Square (RMS) deviation for all the rays traced that reach the focal point. In most cases, the RMS deviation is based on 55, individual, ray traces (all of which make it completely through the optical system) and between five to nine routine calls. The program runtime is much quicker than the fine FORTRAN grid approach. It also takes into account the optical characteristics (such as light divergent angles) of the system, instead of simple surface matching.

The ray pattern, which first "illuminates" the optic, is a hexagonal pattern of light rays. Half are perfectly parallel and half represent solar radiation (1/2 degree divergence angle). Ray data, typical of the input file used, is provided in the Appendix (see BEAM 4 Input, along with Figures 10. to 11.). The physical layout is shown in Figure 10. (page 38), with a corresponding representative focal point image in Figure 10. (page 38). When 10,000 random rays are added (by Monte Carlo numerical routine), the focal plane is filled (see Figure 12. on page 39). The shape seen in that plot is typical of the interior mirror facets. The image shape is much more distorted and wider for facets farther away from the origin. This includes the wide spread, non uniform scatter of even the parallel light rays. Facet Group 14 clearly illustrates this point (see Figures 14. and 15. on page 40) on both its two dimensional and three dimensional focal plots (for a comparison, refer back to page 39, Figures 12. and 13.).

The actual input values for BEAM 4 were arranged so the light ray pattern remained fixed along the Z-axis. The facets were held to the origin, but allowed to pivot in two directions (Tilt and Pitch). The focal point was defined as the negative coordinate value of the actual facet center. Thus, a simple coordinate transformation is used to greatly simplify the setup and execution of each case. No additional error is introduced by use of this methodology. The tabulated results are given in Table 3. under the BEAM 4 heading.

The Pitch and Tilt values, for each facet group (see Figure 9.), are comparable using the different programs. The difference recorded is in the hundredth of a degree. Like the offset values, this is far beyond the solar thermal concentrator's alignment

capability. The random ray generator confirmed the suspicion that the Tilt and Pitch values are not important to the focal spot size, if within a degree or so of proper alignment. There can be significant spot widening and distortion when the mirrors are out of alignment by several degrees.

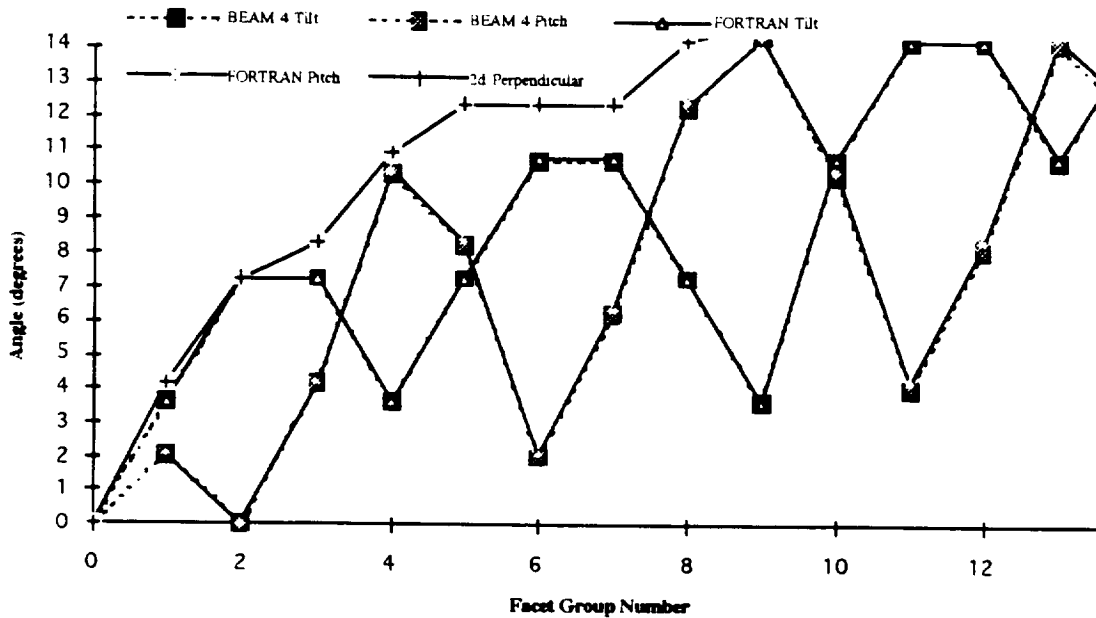


FIGURE 9: TILT AND PITCH ANGLES

The radii of curvature are generally within one half percent of the three dimensional, FORTRAN results (Figure 8.). The last variable of interest is the RMS deviation. However, this value can not be compared side by side with the RMS value generated by our code. BEAM 4 is based on the spread of 55 light rays that ended on the focal plane. The surface matching RMS is based on the linear error of about 5,000 evenly spaced grid points. In the ray trace, the ray pattern is very dependent on the initial user's, selected rays. Hence a different RMS was obtained depending on the number and orientation of start rays. The sunshape, orientation, limb darkening and spectral dependence all exert some influence on the direct incident, solar radiation. Fortunately, the effect of these factors are considered minor, since they could not be ideally represented in the ray trace input.^{5,6}

Besides not being able to directly compare RMS values, the influence of the initial rays creates bias in the curvature optimization. The radius will change over an inch or more depending on what rays and how many are used. The effect would be minimal, if the program was not limited to about 60 evaluation points. The bias was so strong that even the best results from the three dimensional surface matching code would not produce a smaller RMS value, when used in the BEAM 4 program. Nevertheless, these differences were very slight and none had any appreciable effect on the focal spot size. The 10,000 random rays generated identical flux profiles using either of the optimized radius values.

TABLE 5: 2-D FITS IN BEAM 4 CODE

Group	2D Circle Centered				2D Circle Perpendicular			
	Radius	Tilt	Pitch	RMS	Radius	Tilt	Pitch	RMS
1	216.45	3.62	2.09	0.01447	217.64	3.62	2.09	0.01453
2	217.06	7.22	0.00	0.01486	221.20	7.22	0.00	0.01504
4	218.23	3.62	10.34	0.01625	228.54	3.63	10.34	0.05251
9	219.97	3.62	14.33	0.01984	239.43	3.63	14.33	0.01878
12	220.84	14.22	8.07	0.02225	244.92	14.22	8.07	0.02012

3. Two Dimension Results in Three Dimension Reality

The final numerical evaluation was to compare the two dimensional results in the two more advanced (three dimensional) models. Both code inputs were easily changed to accommodate the fixed radii. The pitch and tilt values were left to optimize automatically by the ray trace program. In this way, the three dimensional geometry was checked, but the actual alignment of the facet was considered an external adjustment, that had to be made in all cases. The FORTRAN routine relies on the fixed tangent point geometry, at the center. Therefore, it did not have the tilt and pitch issue to contend with.

The results of the two dimensional analysis were somewhat expected. Using BEAM 4, the two dimensional radii produce a significantly worse energy flux distribution than that of the full, three dimensional solution. The spot size was larger and slightly distorted. In some cases, the results were almost double the size of the full three dimensional solutions (Table 5. has some typical results of the calculations). However, the facets near the center were amazingly accurate. The least accurate, two dimensional, Circle Centered case was less than a one percent difference from the best ray trace calculation, for Group 1 facets. The comparison of the same calculations for Group 12 mirrors were about 19 percent different in their root mean squares. Similar results were seen using the FORTRAN program. In the interest of CPU time, not all groups were rerun for the two dimensional case, in the three dimensional codes.

V. Follow-On Research

Much more research is planned on the solar thermal evaluation. The work is short of what the Propulsion Research Center (PRC) had hoped to accomplish. Primarily the evaluation and high temperature tests using the 10 foot diameter, faceted mirror was not possible, since none of the facets had been polished. One cause was the unfortunate departure of MSFC employee, Steve Fawcett. He had planned to start polishing the facets as soon as the diamond lathe was relocated. Besides this delay at MSFC, the supplier of the cast facets had not manufactured all 60 hexagon plates. They were working on the order, but have been waiting for suitable weather (i.e. proper temperature and humidity). The research started in this contract will be continued (UAH is now picking up all the costs of equipment and materials to continue

the work) as a University project. All future results will be shared with MSFC through the Advanced Concepts Office.

In addition to the direct thermal evaluation of the facets, the mirror system will be assessed, using a laser mapping technique. The faceted mirror will be compared to a four foot, thin-film, mirror. The vacuum formed mirror and the laser mapping apparatus are in place (Figure 17. on the bottom of page 41 in the Appendix). Only preliminary laser mapping has been completed and the process is under refinement. A comparison of our methodology and equipment will be made with that used by SAIC for their Stretched-Membrane Dish.⁷ The mapping will produce contour plots at the focal point, indicating the distortion and concentration characteristics of the concentrator. Light reflectivity and scatter tests are scheduled as well. The process will be repeated for the faceted mirror and the results compared and contrasted. A more sophisticated image sensing calibration device from McDonnell Douglas is being sought to test one or two facets. This device is primarily used for highly accurate, telescope optics and should provide an excellent comparison to our laser mapping of the entire mirror.

The final test, to compare the calculated results, is a focal point image produced by moonlight. This technique was used by Schubnell, et. al., for solar density flux measurements.⁸ In addition to photographic output, the focal point energy distribution will be determined by a "short burst vaporization" procedure. To create a three dimensional, solid image of the energy flux at the focal point, a small block of highly, volatile material, which quickly vaporizes at high temperature, (such as polystyrene plastic) will be used.

The research is expected to expand the various, mirror evaluation methods (discussed above) to characterize other concentrators. Fresnel, vacuum formed, inflatable and rigid are the four major, mirror categories. A sample of each is expected to be evaluated in the coming year. High temperature testing of aluminum, carbon and exotic metal alloys samples are anticipated, when the full concentrator is complete. In addition to the material testing, the geometry and surface characteristics are of extreme interest (particularly the solar energy interactions).

VI. Conclusions and Recommendations

Physical construction of a research solar concentrator was shown to be possible at a relatively inexpensive cost (approximately \$10,000 plus mirror polishing). Casting was shown to work as well as aluminum plate for the facets and was slightly less expensive. Rough cutting the dish surface can be accomplished on a standard lathe, thus saving expensive diamond turning lathe usage. Coatings are advisable, particularly for concentrators that are not totally enclosed, but uncoated mirrors are resistant to dulling over several months when sheltered. Further investigation should be carried out to determine the best coating application.

The frame must be stiff and provide a wide area for facet attachment. Manual adjustment, in all three coordinates, is needed to ensure proper alignment of each facet. Adjustment of the heliostat glass was found to be very helpful in correcting the

imperfections of the glass. The substitution of a thin, fabric-backed mirror was shown to be equal to thick (1/4 inch) plate glass mirror. Mirror silvering is expected to maintain its reflectiveness for a much longer time than standard plate mirror (conformation of this should be demonstrated during the next year of operation).

Vacuum pump capacity is a limiting factor on small thruster testing. Direct thrust measurements are possible but great effort must be made to ensure a proper calibration. Any changes to the mounting or reinstallation of the components in the test chamber will require a calibration check for the load cells.

Having conducted a myriad of comparative computations, the data indicate several important trends and considerations, in a faceted mirror concentrator. The spherical approximation to the parabolic curve is an appropriate methodology to use for these concentrators. However, its practical application (i.e. using the tangent of the surface at the facet center, 3-D instead of 2-D calculations, etc.) is important and can have significant effect upon the focal point size and intensity.

In general, the two dimensional Center Circle approach was simple, but produced poor results for many of the facets in the ten foot concentrator. The Perpendicular approach was much better, producing acceptable radius measurements. Both gave great results for the inner most facets, but lost accuracy for the facets located farther away from the center of the paraboloid. The outer facets, in the 10 foot mirror, would have been unacceptable using the two dimensional radii of curvature. The focal point spot size would have grown between ten and fifteen percent. Thus, for large scale mirrors (greater than eight feet), the more complicated, three dimensional analysis is recommended.

The spherical curve was shown to match the parabolic curve better, when the curves were shifted so they overlapped at two points (instead of the intersection fixed at the center of the facet). The three dimensional geometry also benefited from a shift of the spherical surface (usually away from the faceted center, with a corresponding increase in the radius of curvature). However, in all cases, the optimum shift was exceedingly small and well beyond practical manufacturing tolerances. Thus, the neglect of offsets is justifiable, in the faceted solar collection design.

Optical ray tracing was theoretically considered to be the best approach, for determining radius of curvature, tilt and pitch angles and error estimates. BEAM 4 performed well in these estimates. It also provided excellent focal flux diagrams, which can be utilized in the thermal calculations of a solar absorber. It was a very quick, PC based package and flexible enough to model hexagonal facets, in three dimensions. The weakness is in the limited number of ray traces it can utilize for the optimization process. This made it susceptible to variations of the initial ray distributions used. Optimization of the key parameters suffered, although only slightly in the 10 foot mirror case.

The surface matching algorithm was shown to be extremely accurate. It used significantly more computing power and required double precision accuracy to prevent code errors. However, with some additional code optimization and the elimination of the offset calculations, the code could be much more efficient to run. The best facet tilt and pitch angles were demonstrated to lie on the tangent lines to the paraboloid surface, at the facet center.

Even though the facets were always found to have greater deviation error, the farther they were from the concentrator center, the three dimensional codes were able to determine a highly accurate, optimal radius of curvature. For the 10 foot mirror, all facets had satisfactory results, which corresponded to a tight focal point. The extrapolation to larger mirrors appears very practical. Lengthening the focal distance should also improve the outer facets' surface approximation.

The program was successful in obtaining practical knowledge of concentrator fabrication. Use of the information can be directly applied to the design and construction of a full scale, solar thermal, ground test facility at MSFC. The available components from this research should continue to be assemble into a small facility at UAH and provide small scale, component testing and fundamental research.

References

1. Williams, J. Richards, Solar Energy Technology and Applications, Ann Arbor Science Publishers, Inc., Ann Arbor, Michigan, 1974.
2. Bradford, R., Research on Large, Highly Accurate, Inflatable Reflectors, AFRPL TR-84-040, Final Report, Air Force Rocket Propulsion Laboratory, Edwards Air Force Base, California, July, 1984.
3. Bonometti, J.A. and Hawk, C.W., Solar Thermal Research Facility Design, AIAA Paper No. 94-3028; June 1994.
4. Lampton, Michael, BEAM 4 Optical Ray Tracer, Stellar Software, Berkeley, California, 1989.
5. Schubnell, M., "Sunshape and Its Influence on the Flux Distribution in Imaging Solar Concentrators," Journal of Solar Energy Engineering, Vol. 114, pp. 260-266, November 1992.
6. Rabl, Ari, Active Solar Collectors and Their Applications, Oxford University Press, Inc., New York, New York, 1985, pp. 170-211.
7. Science Applications International Corporation, Energy Projects Division, Contractor Report / Facet Development for a Faceted Stretched-Membrane Dish by SAIC, San Diego, California, October 1991.
8. Schubnell, M., Keller, J. and Imhof, A., "Flux Density Distribution in the Focal Region of a Solar Concentrator System," Journal of Solar Energy Engineering, pp. 112-116, May 1991.

Appendix

FORTRAN Code

HEXAGONAL FACET MATCHING ALGORITHM

Program for mirror facet curve using rms deviation.
Spherical approximation to a parabolic surface.
Written by Joe Bonometti 6/28/95

```
and Jmax must be equal!
parameter (imax=75,jmax=75,kmax=2)
common/coor/x(imax,jmax,kmax),y(imax,jmax,kmax),z(imax,jmax,kmax)
common xp(imax,jmax),yp(imax,jmax),zp(imax,jmax)
common xs(imax,jmax),ys(imax,jmax),zs(imax,jmax)
common/tag/mtag(imax,jmax)
data pi/3.141592654/
open(1,file='c.inp',status='old')
read(1,*) s,thick,fl,radstart,radfin,nradii,nhshifts,
         cx,cy,cz,nfc

Hexagon side length in inches
s - plate thickness (inches)
fl - focal length of parabolic mirror (inches)
radstart - circle radius minimum or starting value
radfin - circle radius maximum or ending value
nradii - number of radii to try between the min and max values
         (pick an even integer)
nhshifts - number of radii shifts (-1) in half the plate thickness
           (use an odd integer or negative number to by-pass)
cx,cy,cz - 3D coordinates for the center of the facet
nfc - number of facet cases to follow (=0 for one case, =1 for two...)
       (sets of 3 coord. values follow for each extra facet case)

open(18,file='cdata1.out',status='unknown')
open(19,file='cdata2.out',status='unknown')
open(20,file='cdata3.out',status='unknown')
write(20,(''FACET OPTIMIZATION {rms}''))
write(20,*) s,thick,fl,radstart,radfin,nradii,nhshifts,nfc
write(20,*)
RADIUS      rms      TILT      PITCH*
Program is run for several cases at once (i.e. nfc > 0), no plotting
is generated and only the final values are printed to cdata.out
ncase=1,(nfc+1)
do(ncase.gt.1) read(1,*) cx,cy,cz
               cumulative values
               mbest=10000.0
               lbest=10000.0
               lcumbest=10000.0
               counter=0.0
               facet case...
               try
               *****
               selection is set to work for a hexagon ONLY!! (careful code review
               needed if the shape or orientation is required to be changed)
               =6.0
               s/(2.0*(tan(pi/sn)))
               =s

               a square for the grid that fits the hex inside
               1,1,1)=-rr
               1,1,1)=-rr
               lta=(2.*rr)/float(imax-1)
               j=1,jmax
```

```

do i=1,imax
  x(i,j,1)=x(1,1,1)+float(i-1)*delta
  x(i,j,2)=x(i,j,1)
  y(i,j,1)=y(1,1,1)+float(j-1)*delta
  y(i,j,2)=y(i,j,1)
C Check if point is inside facet (if yes, z=thick/2, if no, z=-thick/2)
C In the box?
  if(x(i,j,1).ge.-r.and.x(i,j,1).le.r.and.
    >y(i,j,1).ge.-(s/2.).and.y(i,j,1).le.(s/2.)) go to 100
C No, check corners
  if(y(i,j,1).gt.(s/2.)) go to 50
  if(x(i,j,1).gt.0.0) go to 60
C Bottom left
  s1=(0.5*s)/(-r)
  b1=-s
  yline=s1*x(i,j,1)+b1
  if(y(i,j,1).ge.yline.and.x(i,j,1).ge.-r) go to 100
  go to 110
C Bottom right
60 s1=(0.5*s)/r
  b1=-s
  yline=s1*x(i,j,1)+b1
  if(y(i,j,1).ge.yline.and.x(i,j,1).le.r) go to 100
  go to 110
C
50 if(x(i,j,1).lt.0.0) go to 70
C Top right
  s1=(0.5*s)/(-r)
  b1=s
  yline=s1*x(i,j,1)+b1
  if(y(i,j,1).le.yline.and.x(i,j,1).le.r) go to 100
  go to 110
C Top left
70 s1=(0.5*s)/r
  b1=s
  yline=s1*x(i,j,1)+b1
  if(y(i,j,1).le.yline.and.x(i,j,1).ge.-r) go to 100
  go to 110
C
100 continue
  z(i,j,1)=-thick/2.
  z(i,j,2)=thick/2.
  mtag(i,j)=1
  counter=counter+1.
  go to 120
110 continue
  z(i,j,1)=-thick/2.
  z(i,j,2)=-thick/2.
  mtag(i,j)=0

120 continue
end do
end do
C
  ex=0.
  ey=0.
  ez=thick/2.
C
C Tilt facet to tangent of parabola
C Tangent slope in y-z plane is dy/dz
C Transfer Rectangular to Polar coordinates, rotate them by adding tslope,
C and convert back again
  if(cy.eq.0.0) go to 200

```

```

dydz=2.0*f1/cy
tslope=ATAN(dydz)
tilt=90.-(tslope*180./pi)
do k=1,2
do j=1,jmax
do i=1,imax
theta=ATAN(y(i,j,k)/z(i,j,k))
if(z(i,j,k).lt.0.0) theta=pi+theta
if(y(i,j,k).lt.0.0.and.z(i,j,k).gt.0.0) theta=(2.*pi)+theta
rcoord=SQRT((y(i,j,k)**2.)+(z(i,j,k)**2.))
thetanew=theta-((pi/2.0)-tslope)
if(thetanew.lt.0.0) thetanew=(2.*pi)+thetanew
z(i,j,k)=rcoord*COS(thetanew)
y(i,j,k)=rcoord*SIN(thetanew)
end do
end do
end do
C
theta=ATAN(ey/ez)
if(ez.lt.0.0) theta=pi+theta
if(ey.lt.0.0.and.ez.gt.0.0) theta=(2.*pi)+theta
rcoord=SQRT((ey**2.)+(ez**2.))
thetanew=theta-((pi/2.0)-tslope)
if(thetanew.lt.0.0) thetanew=(2.*pi)+thetanew
ez=rcoord*COS(thetanew)
ey=rcoord*SIN(thetanew)
C
200 continue
C
C Tangent slope in x-z plane is dx/dz
C Transfer Rectangular to Polar coordinates, rotate them by adding tslope,
C and convert back again
if(cx.eq.0.0) go to 210
dxdz=2.0*f1/cx
tslope=ATAN(dxdz)
pitch=90.-(tslope*180./pi)
do k=1,2
do j=1,jmax
do i=1,imax
theta=ATAN(x(i,j,k)/z(i,j,k))
if(z(i,j,k).lt.0.0) theta=pi+theta
if(x(i,j,k).lt.0.0.and.z(i,j,k).gt.0.0) theta=2.*pi+theta
rcoord=SQRT((x(i,j,k)**2.)+(z(i,j,k)**2.))
thetanew=theta-((pi/2.0)-tslope)
z(i,j,k)=rcoord*COS(thetanew)
x(i,j,k)=rcoord*SIN(thetanew)
end do
end do
end do
C
theta=ATAN(ex/ez)
if(ez.lt.0.0) theta=pi+theta
if(ex.lt.0.0.and.ez.gt.0.0) theta=2.*pi+theta
rcoord=SQRT((ex**2.)+(ez**2.))
thetanew=theta-((pi/2.0)-tslope)
ez=rcoord*COS(thetanew)
ex=rcoord*SIN(thetanew)
C
210 continue
C
C Center coordinate transformation

```

```

C Volume center of facet is set on parabolic curve
  do j=1,jmax
  do i=1,imax
  x(i,j,1)=x(i,j,1)+cx
  y(i,j,1)=y(i,j,1)+cy
  z(i,j,1)=z(i,j,1)+cz
  x(i,j,2)=x(i,j,2)+cx
  y(i,j,2)=y(i,j,2)+cy
  z(i,j,2)=z(i,j,2)+cz
  end do
  end do
C
  ex=ex+cx
  ey=ey+cy
  ez=ez+cz
C
C Calculate the parabolic curve z coordinates
C *****
  do j=1,jmax
  do i=1,imax
  if(mtag(i,j).eq.0) go to 300
C Knowing 2 points, calculate parametric equation
C constants, a, b and c for the line (which so happens to be perpendicular
C to the parabolic tangent plane!)
  ape=x(i,j,2)-x(i,j,1)
  bpe=y(i,j,2)-y(i,j,1)
  cpe=z(i,j,2)-z(i,j,1)
  cona=1.+(ape/bpe)**2.
  conb=(2.*(ape/bpe))*(x(i,j,1)-(y(i,j,1)*(ape/bpe)))
  >-(4.*fl*(cpe/bpe))
  concl=((ape/bpe)*y(i,j,1))**2.
  conc2=-((2.*x(i,j,1)*y(i,j,1)*(ape/bpe))
  conc3=x(i,j,1)**2.+(4.*fl*y(i,j,1)*(cpe/bpe))-(4.*fl*z(i,j,1))
  conc=concl+conc2+conc3
C
C The solution of the quadratic equation assumes the y coordinate is
C positive, which is true for the first quadrant facets
  yp(i,j)=(-conb+SQRT(conb**2.-(4.*cona*conc)))/(2.*cona)
  xp(i,j)=(yp(i,j)*(ape/bpe))-(y(i,j,1)*(ape/bpe))+x(i,j,1)
  zp(i,j)=(yp(i,j)*(cpe/bpe))-(y(i,j,1)*(cpe/bpe))+z(i,j,1)
C Check if solution is close
  zcheck=((xp(i,j)**2.)+(yp(i,j)**2.))/(4.*fl)
  if((abs(zcheck-zp(i,j))*100./zp(i,j)).gt.
  >0.1) write(*,*) "parabola error"
C
  300 continue
  end do
  end do
C
C Print initial information
  write(18,*) tilt,pitch
  write(19,*) tilt,pitch
C
C Calculate the spherical approximate curve coordinates for each
C facet point, compare to parabolic point and sum error
C *****
  radincr=(radfin-radstart)/float(nradii-1)
  do loop=1,nradii
  radius=radstart+radincr*float(loop-1)
C
C The line perpendicular to the parabola tangent line is the radius

```

```

the circle (i.e. center normal line)
and the sphere's center coordinates sx,sy,sz
  if(cy.ne.0.) go to 320
  sx=cx
  sy=cy
  sz=radius
  go to 310
  bigcon=1+((ex-cx)/(ey-cy))**2.+((ez-cz)/(ey-cy))**2.
  conaa=bigcon
  conbb=-2.*cy*bigcon
  concc=cy**2.*bigcon-radius**2.
  sy=(-conbb-SQRT(conbb**2.-4.*conaa*concc))/(2.*conaa)
  sx=((sy-cy)*(ex-cx)/(ey-cy))+cx
  sz=((sy-cy)*(ez-cz)/(ey-cy))+cz
back of results
  rcheck=SQRT((cx-sx)**2.+(cy-sy)**2.+(cz-sz)**2.)
  if((abs(rcheck-radius)*100./radius).gt.0.1) write(*,*) "center 1"

calculate the spherical curve x,y,z coordinates, xs(i,j),ys(i,j),zs(i,j)
total error at all points
  cumerror=0.0
  do j=1,jmax
  do i=1,imax
  if(mtag(i,j).eq.0) go to 400
  wing 2 points, calculate parametric equation
  constants, a, b and c for the line (which so happens to be perpendicular
  the facet's plate plane!)
  ape=x(i,j,2)-x(i,j,1)
  bpe=y(i,j,2)-y(i,j,1)
  cpe=z(i,j,2)-z(i,j,1)
  cona=1.+(ape/bpe)**2.+(cpe/bpe)**2.
  conb=2*((z(i,j,1)*(cpe/bpe))-y(i,j,1)*(cpe/bpe))**2.+
  >x(i,j,1)*(ape/bpe)-y(i,j,1)*(ape/bpe))**2.-
  >sz*(cpe/bpe)-sx*(ape/bpe)-sy)
  conc=sx**2.+sy**2.+sz**2.-radius**2.+
  >2.*sx*y(i,j,1)*(ape/bpe)-2.*sx*x(i,j,1)+2.*sz*y(i,j,1)*(cpe/bpe)-
  >2.*sz*z(i,j,1)+(y(i,j,1)*(ape/bpe))**2.-2*y(i,j,1)*x(i,j,1)*
  >(ape/bpe)+x(i,j,1)**2.+(y(i,j,1)*(cpe/bpe))**2.-2*y(i,j,1)*
  >z(i,j,1)*(cpe/bpe)+z(i,j,1)**2.

solution of the quadratic equation assumes the y coordinate is
positive, which is true for the first quadrant facets
  ys(i,j)=(-conb+SQRT(conb**2.-4.*conaa*concc))/(2.*conaa)
  xs(i,j)=(ys(i,j)*(ape/bpe))-y(i,j,1)*(ape/bpe)+x(i,j,1)
  zs(i,j)=(ys(i,j)*(cpe/bpe))-y(i,j,1)*(cpe/bpe)+z(i,j,1)
back if solution is close
values are considered always positive and the sphere's solution
is less than the sz value (sphere center z coordinate)
  zcheck=radius**2.-(xs(i,j)-sx)**2.-(ys(i,j)-sy)**2.
  zcheck=-SQRT(zcheck)+sz
  if((abs(zcheck-zs(i,j))*100./zs(i,j)).gt.
  >2.0) write(*,*) "circle 1"

calculate the distance between two points
the parabolic and spherical)
  diff1=SQRT((xs(i,j)-xp(i,j))**2.+
  >(ys(i,j)-yp(i,j))**2.+(zs(i,j)-zp(i,j))**2)
  cumerror=cumerror+(diff1**2.)
) continue
end do
end do

```

```

rmserror=SQRT(cumerror/counter)

: the best radius case
if(rmserror.lt.cumbest) radbest=radius
if(rmserror.lt.cumbest) cumbest=rmserror

: print each result
write(18,*) radius,rmserror

: check offsets for this radius
*****

: pass
if(nhshifts.lt.0) go to 500
adjust the sphere's contact point to the facet center,
: radius is modified over the range of the facet thickness
: in many cases were evaluated, the results indicated that
: a shift distance was very small. Therefore, the 0.0001 factor
: is placed in the next line.
rmodinc=thick*0.001/(2.*float(nhshifts))
do loopmod=1,(nhshifts*2-1)
if(loopmod.lt.nhshifts) raddelta=rmodinc*float(nhshifts-loopmod)
if(loopmod.ge.nhshifts) raddelta=-rmodinc*float(loopmod-nhshifts)

: find the sphere's center coordinates sx,sy,sz
if(raddelta.eq.0.) go to 460
sxo=sx
syo=sy
szo=sz
bigcon=1+((cx-sxo)/(cy-syo))**2.+((cz-szo)/(cy-syo))**2.
conaa=bigcon
conbb=-2.*syo*bigcon
concc=syo**2.*bigcon-raddelta**2.
if(raddelta.lt.0.) sign=1.
if(raddelta.ge.0.) sign=-1.
syn=(-conbb+(sign*SQRT(conbb**2.-(4.*conaa*concc))))/(2.*conaa)
sxn=((cx-sxo)*(syn-syo)/(cy-syo))+sxo
szn=((cz-szo)*(syn-syo)/(cy-syo))+szo
go to 470
continue

: eliminate round off errors when raddelta is 0
sxn=sx
syn=sy
szn=sz
continue

: check of results
dcheck=SQRT((ex-sxn)**2.+(ey-syn)**2.+(ez-szn)**2.)
rchk=radius-(thick/2.)+raddelta
if((abs(rchk-dcheck))*100./rchk.gt.
>0.1) write(*,*) "center 2"

: calculate the spherical curve x,y,z coordinates, xs(i,j),ys(i,j),zs(i,j)
total error at all points
cumerr=0.0
do j=1,jmax
do i=1,imax
if(mtag(i,j).eq.0) go to 401
: using 2 points, calculate parametric equation
: constants, a, b and c for the line (which so happens to be perpendicular
: to the facet's plate plane!)
ape=x(i,j,2)-x(i,j,1)

```

```

    bpe=y(i,j,2)-y(i,j,1)
    cpe=z(i,j,2)-z(i,j,1)
    cona=1.+(ape/bpe)**2.+(cpe/bpe)**2.
    conb=2*((z(i,j,1)*(cpe/bpe))-y(i,j,1)*(cpe/bpe)**2.+
>x(i,j,1)*(ape/bpe)-y(i,j,1)*(ape/bpe)**2.-
>szn*(cpe/bpe)-sxn*(ape/bpe)-syn)
    conc=sxn**2.+syn**2.+szn**2.-radius**2.+
>2.*sxn*y(i,j,1)*(ape/bpe)-2.*sxn*x(i,j,1)+2.*szn*y(i,j,1)*(cpe/
>bpe)-2.*szn*z(i,j,1)+(y(i,j,1)*(ape/bpe))**2.-2*y(i,j,1)*x(i,j,1)
>*(ape/bpe)+x(i,j,1)**2.+(y(i,j,1)*(cpe/bpe))**2.-2*y(i,j,1)*
>z(i,j,1)*(cpe/bpe)+z(i,j,1)**2.
C
C The solution of the quadratic equation assumes the y coordinate is
C positive, which is true for the first quadrant facets
    ys(i,j)=(-conb+SQRT(conb**2.-(4.*cona*conc)))/(2.*cona)
    xs(i,j)=(ys(i,j)*(ape/bpe))-(y(i,j,1)*(ape/bpe))+x(i,j,1)
    zs(i,j)=(ys(i,j)*(cpe/bpe))-(y(i,j,1)*(cpe/bpe))+z(i,j,1)
C Check if solution is close
C Z values are considered always positive and the sphere's solution
C less than the sz value (sphere center z coordinate)
    zcheck=radius**2.-(xs(i,j)-sxn)**2.-(ys(i,j)-syn)**2.
    zcheck=-SQRT(zcheck)+szn
    if((abs(zcheck-zs(i,j))*100./zs(i,j)).gt.
>0.1) write(*,*) "circle 2"
C
C Calculate the distance between two points (the parabolic and spherical)
    diff2=SQRT((xs(i,j)-xp(i,j))**2+
>(ys(i,j)-yp(i,j))**2+(zs(i,j)-zp(i,j))**2)
    cumerr=cumerr+diff2**2.
401 continue
    end do
    end do
    rmserr=SQRT(cumerr/counter)
C
C Print each result
    write(19,*) radius,raddelta,rmserr

C Save the best case
    if(rmserr.lt.delcumbest) delradbest=radius
    if(rmserr.lt.delcumbest) delbest=raddelta
    if(rmserr.lt.delcumbest) delcumbest=rmserr
C Go back and get next shift point
    end do
C By-pass ends
500 continue
C
C Get new radius
    end do
C
C Print the best case for with and without shift
    write(20,*) radbest,cumbest,tilt,pitch
    If(nhshifts.ge.0) write(20,*) delradbest,delbest,delcumbest
C
C Go back for other cases if any
    end do
    if(nfc.gt.0) go to 999
C
C
    call plot (radbest,fl,pi,s,sx,sy,sz,cx,cy)
C
920 format(F7.4,2x,F7.4,F8.5,2x,F8.4,2x,F8.4,2x,
>F10.5,2x,E12.5,2x,F10.6)

```



```

C
  999 continue
  end
  SUBROUTINE plot (radbest,fl,pi,s,sx,sy,sz,cx,cy)
C Imax and Jmax must be equal!
  parameter (imax=75,jmax=75,kmax=2)
  common/coor/x(imax,jmax,kmax),y(imax,jmax,kmax),z(imax,jmax,kmax)
  common/tag/mtag(imax,jmax)
C
  open(2,file='c.out',status='unknown')
  write(2,(''TITLE = "Mirror Facet Points"''))
  write(2,(''VARIABLES = "X", "Y", "Z", "tag"''))
C Do not forget to change this line when changing the number of points
C in the parameter statement.
  write(2,(''ZONE T="Facet", I=75, J=75, K=2, F=POINT''))
C
C Facet plot output, Zone1
  do j=1,jmax
  do i=1,imax
  write(2,900) x(i,j,1),y(i,j,1),z(i,j,1),mtag(i,j)
  end do
  end do
C
  do j=1,jmax
  do i=1,imax
  write(2,900) x(i,j,2),y(i,j,2),z(i,j,2),mtag(i,j)
  end do
  end do
C
C Parabolic curve plot output, Zone 2
  write
  >(2,(''ZONE T="PARABOLA", I=25, J=25, K=1, C=YELLOW, F=POINT''))
C Define a grid square that fits the parabolic curve in the first quad.
C Select the grid max distance (inches) as an whole number
C **** Also set the write statement above for I and J! ****
  grid=50.0
  ngrid=ifix(grid/2.0)
  delta=grid/float(ngrid-1)
  adel=pi/2.0/float(ngrid-1)
  do j=1,ngrid
  ang=adel*float(j-1)
  do i=1,ngrid
  hdis=delta*float(i-1)
  xpar=hdis*cos(ang)
  ypar=hdis*sin(ang)
  zpar=(xpar**2.+ypar**2.)/(4.*fl)
  write(2,910) xpar,ypar,zpar,1
  end do
  end do
C
C Best sphere plot output, Zone 3
  write
  >(2,(''ZONE T="SPHERE", I=25, J=25, K=1, C=BLUE, F=POINT''))
C Define a grid that approximates the best spherical curve in the first quad.
C Select the number of grid points as an whole number
C **** Also set the write statement above for I and J! ****
  ngrid=25
  delta=(6.*s)/FLOAT(ngrid-1)
  xstart=cx-(3.*s)
  ystart=cy-(3.*s)
  do j=1,ngrid

```

```
    ysph=ystart+delta*FLOAT(j-1)
    do i=1,ngrid
: Pick where x and y coordinates are to represent the sphere,
: then calculate the z coordinate from the 3-D spherical equation.
        xsph=xstart+delta*FLOAT(i-1)
        zsph=-SQRT(radbest**2-(xsph-sx)**2-(ysph-sy)**2)+sz
        write(2,910) xsph,ysph,zsph,1
    end do
end do
:
900 format(3F10.3,1I3)
910 format(3F8.2,1I3)
RETURN
end
```

FORTRAN Input

9.125
0.1
108.0
230.9
231.4
500
-1
55.31737267
13.6875
7.51703559
0

7.90248181
13.6875
0.578233507
0.
27.375
1.734700521
15.80496362
27.375
2.312934028
39.5124095
13.6875
4.047534549
31.60992724
27.375
4.047634549
7.90248181
41.0625
4.047634549
23.70744543
41.0625
5.204101563
47.41489086
27.375
6.938802083

39.51240905
41.0625
7.51703559
15.80496362
54.75
7.51703559
31.60992724
54.75
9.251736111
55.31737267
41.0625
10.98643663
47.41489086
54.75
12.14290365

FORTRAN Output

10.76372735001, 6.263524267702
226., 5.1279923528999E-3
226.001002004, 5.127981829143E-3
226.002004008, 5.1279713364753E-3
226.003006012, 5.1279608749495E-3
226.004008016, 5.1279504443741E-3
226.00501002, 5.1279400449644E-3
226.006012024, 5.1279296766336E-3
226.0070140281, 5.1279193392899E-3
226.0080160321, 5.1279090331341E-3
226.0090180361, 5.1278987580458E-3
226.0100200401, 5.1278885140123E-3
226.0110220441, 5.1278783010153E-3
226.0120240481, 5.1278681191029E-3
226.0130260521, 5.1278579681867E-3
226.0140280561, 5.1278478484289E-3
226.0150300601, 5.1278377597294E-3
226.0160320641, 5.1278277021228E-3
226.0170340681, 5.1278176755222E-3
226.0180360721, 5.1278076800919E-3
226.0190380762, 5.1277977155501E-3
226.0200400802, 5.1277877822319E-3
226.0210420842, 5.1277778799233E-3
226.0220440882, 5.1277680086098E-3
226.0230460922, 5.127758168464E-3
226.0240480962, 5.1277483593835E-3
226.0250501002, 5.127738581379E-3
226.0260521042, 5.1277288342836E-3
226.0270541082, 5.1277191183066E-3
226.0280561122, 5.127709433378E-3
226.0290581162, 5.1276997796475E-3
226.0300601202, 5.1276901569208E-3
226.0310621242, 5.1276805652505E-3
226.0320641283, 5.1276710046429E-3
226.0330661323, 5.1276614749532E-3
226.0340681363, 5.1276519763508E-3
226.0350701403, 5.1276425088472E-3
226.0360721443, 5.1276330724826E-3
226.0370741483, 5.1276236671222E-3
226.0380761523, 5.1276142928666E-3
226.0390781563, 5.1276049496056E-3
226.0400801603, 5.1275956374011E-3
226.0410821643, 5.1275863561893E-3
226.0420841683, 5.1275771060278E-3
226.0430861723, 5.1275678869926E-3
226.0440881764, 5.1275586990442E-3
226.0450901804, 5.1275495421498E-3
226.0460921844, 5.1275404162364E-3
226.0470941884, 5.1275313212953E-3
226.0480961924, 5.12752225746E-3

BEAM 4 Input

6 surfaces		FACET4.OPT		Pitch	Rol	Tilt	Curv	Mir/ln	F	Shp
DY	DX	Kvx	Yvx							
1.6:	:	:	20.0	:	:	:	:	:	:	:
1.5:1.2990381:	:	:	0.06	-10.3432e0.0:	:	3.6249e	:	Iris : c :	:	:
1.5:1.2990381:	:	:	0.04	-10.3432e60.:	:	3.6249e	:	Iris : s :	:	:
1.5:1.2990381:	:	:	0.02	-10.3432e-60:	:	3.6249e	:	Iris : s :	:	:
1.6:	:	:	0.0	-10.34327 0:	:	3.6249?	0.053817	Mirror: c :1.0:	:	:
2.5:	-3.292701:-1.14063:	8.662697:	:	:	:	:	:	Exit : c :	:	:

rms low = .015788 in string @ qcm1

FACET GROUP NUMBER 4
RADIUS=223.006876 INCHES
73 rays

FACET4.RAY

xf	UO yf	VO	WO	Xgoal	Ygoal	Zgoal	ZO	XO	YO	notes
0.0										
0.001:-0.042:		-0.0044999848117486:-0.999989875017089:-3.2927008:-1.140625:8.6626971:215.6652717:					0.0000:	0.930	:ok	6:
0.0012990469254133:-0.0037499957805168:-0.999992124973358:-3.2927008:-1.140625:8.6626971:215.6652717:-0.2685:							0.775	:ok	6:	
0.013:-0.035:										
0.0025980938507226:-0.0029999966242932:-0.99999212493329 :-3.2927008:-1.140625:8.6626971:215.6652717:-0.5369:							0.620	:ok	6:	
0.026:-0.028:										
0.0038970836211076:-0.0022499924060281:-0.999989875085455:-3.2927008:-1.140625:8.6626971:215.6652717:-0.8054:							0.465	:ok	6:	
0.039:-0.021:										
0.0038970923895162:-0.0007499991561646:-0.999992125055079:-3.2927008:-1.140625:8.6626971:215.6652717:-0.8054:							0.155	:ok	6:	
0.039:-0.006:										
0.0038970923895162: 0.0007499991561646:-0.999992125055079:-3.2927008:-1.140625:8.6626971:215.6652717:-0.8054:-0.155							:ok	6:		
0.039: 0.008:										
0.0038970836211076: 0.0022499924060281:-0.999989875085455:-3.2927008:-1.140625:8.6626971:215.6652717:-0.8054:-0.465							:ok	6:		
0.039: 0.022:										
0.0025980938507226: 0.0029999966242932:-0.99999212493329 :-3.2927008:-1.140625:8.6626971:215.6652717:-0.5369:-0.620							:ok	6:		
0.027: 0.029:										
0.0012990469254133: 0.0037499957805168:-0.999992124973358:-3.2927008:-1.140625:8.6626971:215.6652717:-0.2685:-0.775							:ok	6:		
0.014: 0.036:										
0.0		0.0044999848117486:-0.999989875017089:-3.2927008:-1.140625:8.6626971:215.6652717:					0.0000:-0.930	:ok	6:	
0.002: 0.043:										
-0.0012990469254133: 0.0037499957805168:-0.999992124973358:-3.2927008:-1.140625:8.6626971:215.6652717:							0.2685:-0.775	:ok	6:	
0.011: 0.036:										
-0.0025980938507226: 0.0029999966242932:-0.99999212493329 :-3.2927008:-1.140625:8.6626971:215.6652717:							0.5369:-0.620	:ok	6:	
0.024: 0.029:										
-0.0038970836211076: 0.0022499924060281:-0.999989875085455:-3.2927008:-1.140625:8.6626971:215.6652717:							0.8054:-0.465	:ok	6:	
0.037: 0.021:										
-0.0038970923895162: 0.0007499991561646:-0.999992125055079:-3.2927008:-1.140625:8.6626971:215.6652717:							0.8054:-0.155	:ok	6:	
0.037: 0.007:										
-0.0038970923895162:-0.0007499991561646:-0.999992125055079:-3.2927008:-1.140625:8.6626971:215.6652717:							0.8054: 0.155	:ok	6:	
0.037:-0.007:										
-0.0038970836211076:-0.0022499924060281:-0.999989875085455:-3.2927008:-1.140625:8.6626971:215.6652717:							0.8054: 0.465	:ok	6:	
0.037:-0.021:										
-0.0025980938507226:-0.0029999966242932:-0.99999212493329 :-3.2927008:-1.140625:8.6626971:215.6652717:							0.5369: 0.620	:ok	6:	
0.025:-0.028:										
-0.0012990469254133:-0.0037499957805168:-0.999992124973358:-3.2927008:-1.140625:8.6626971:215.6652717:							0.2685: 0.775	:ok	6:	
0.012:-0.035:										
0.0		-0.0030000067494706:-0.999995499969626:-3.2927008:-1.140625:8.6626971:215.6652717:					0.0000: 0.620	:ok	6:	
0.001:-0.028:										
0.0012990527711508:-0.0022500075933442:-0.999996624958168:-3.2927008:-1.140625:8.6626971:215.6652717:-0.2685:							0.465	:ok	6:	
0.013:-0.021:										
0.002598102619314 :-0.0015000033746552:-0.999995499916202:-3.2927008:-1.140625:8.6626971:215.6652717:-0.5369:							0.310	:ok	6:	
0.026:-0.014:										
0.0025981055421975: 0.0										
0.026: 0.001:										
0.002598102619314 : 0.0015000033746552:-0.999995499916202:-3.2927008:-1.140625:8.6626971:215.6652717:-0.5369:							0.000	:ok	6:	
0.027: 0.015:										
0.0012990527711508: 0.0022500075933442:-0.999996624958168:-3.2927008:-1.140625:8.6626971:215.6652717:-0.5369:-0.310							:ok	6:		
0.014: 0.022:										
0.0		0.0030000067494706:-0.999995499969626:-3.2927008:-1.140625:8.6626971:215.6652717:					0.0000:-0.620	:ok	6:	
0.001: 0.029:										
-0.0012990527711508: 0.0022500075933442:-0.999996624958168:-3.2927008:-1.140625:8.6626971:215.6652717:							0.2685:-0.465	:ok	6:	
0.011: 0.022:										
-0.002598102619314 : 0.0015000033746552:-0.999995499916202:-3.2927008:-1.140625:8.6626971:215.6652717:							0.5369:-0.310	:ok	6:	
0.024: 0.014:										
-0.0025981055421975: 0.0										
0.024: 0.000:										
0.002598102619314 : 0.0015000033746552: 0.999995499916202:-3.2927008:-1.140625:8.6626971:215.6652717:							0.5369: 0.310	:ok	6:	
0.025:-0.014:										
-0.0012990527711508:-0.0022500075933442:-0.999996624958168:-3.2927008:-1.140625:8.6626971:215.6652717:							0.2685: 0.465	:ok	6:	
0.012:-0.021:										
0.0		-0.0015000084372951:-0.999998874986711:-3.2927008:-1.140625:8.6626971:215.6652717:					0.0000: 0.310	:ok	6:	
0.001:-0.014:										
0.0012990556940491:-0.0007500042186375:-0.999998874973355:-3.2927008:-1.140625:8.6626971:215.6652717:-0.2685:							0.155	:ok	6:	
0.014:-0.007:										
0.0012990556940491: 0.0007500042186375:-0.999998874973355:-3.2927008:-1.140625:8.6626971:215.6652717:-0.2685:-0.155							:ok	6:		
0.014: 0.008:										
0.0		0.0015000084372951:-0.999998874986711:-3.2927008:-1.140625:8.6626971:215.6652717:					0.0000:-0.310	:ok	6:	
0.001: 0.015:										
-0.0012990556940491: 0.0007500042186375:-0.999998874973355:-3.2927008:-1.140625:8.6626971:215.6652717:							0.2685:-0.155	:ok	6:	
0.012: 0.007:										
-0.0012990556940491:-0.0007500042186375:-0.999998874973355:-3.2927008:-1.140625:8.6626971:215.6652717:							0.2685: 0.155	:ok	6:	
0.012:-0.007:										

BEAM 4 Output

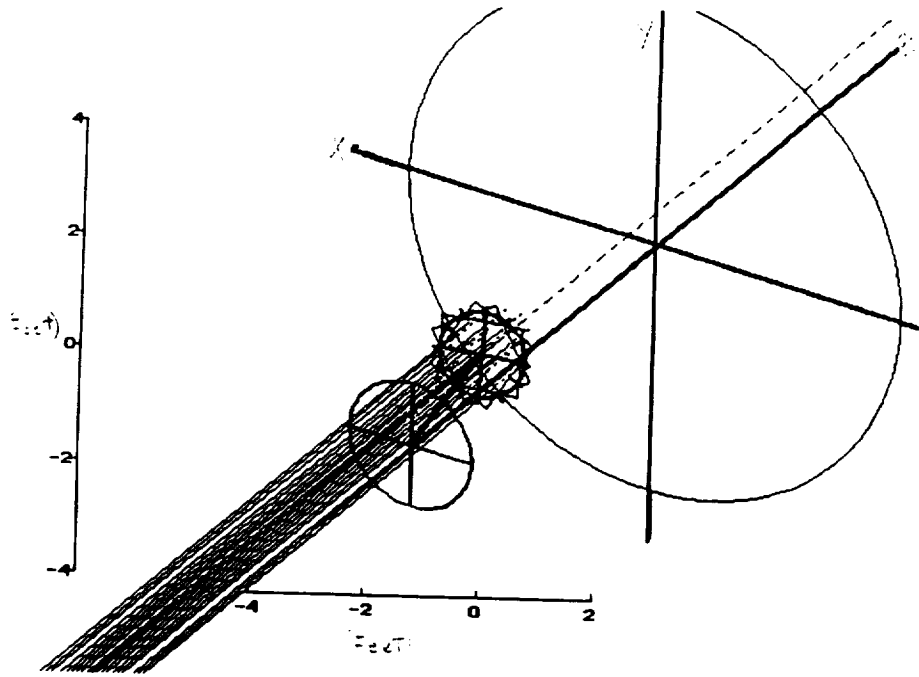


FIGURE 10: BEAM 4 LAYOUT

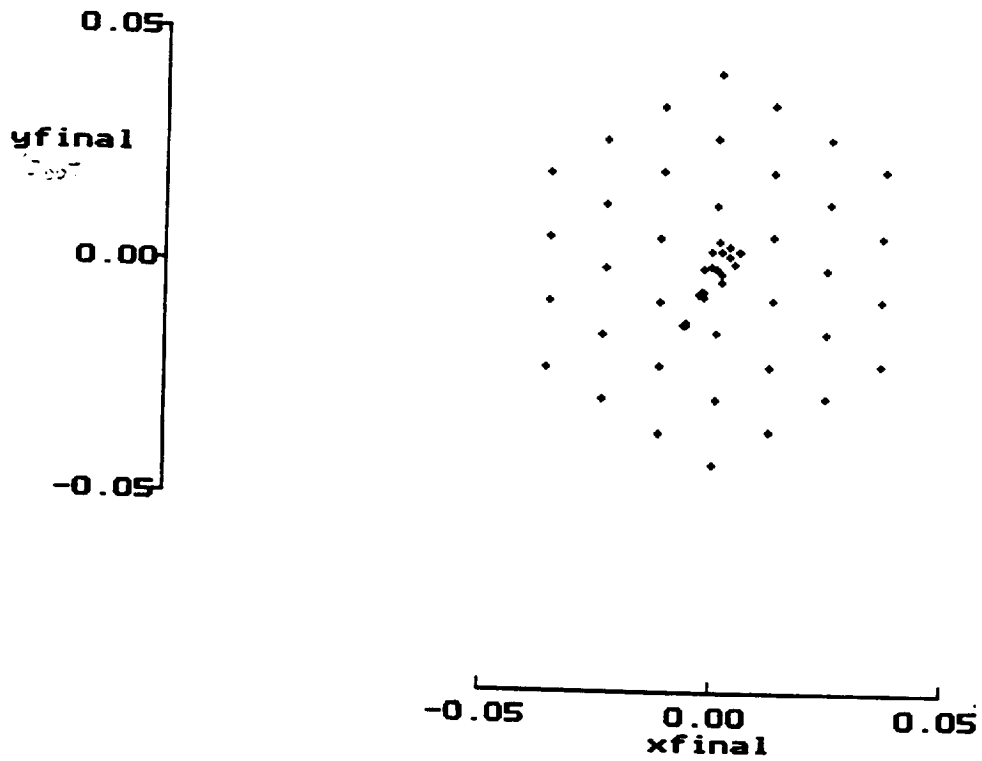


FIGURE 11: FOCAL IMAGE

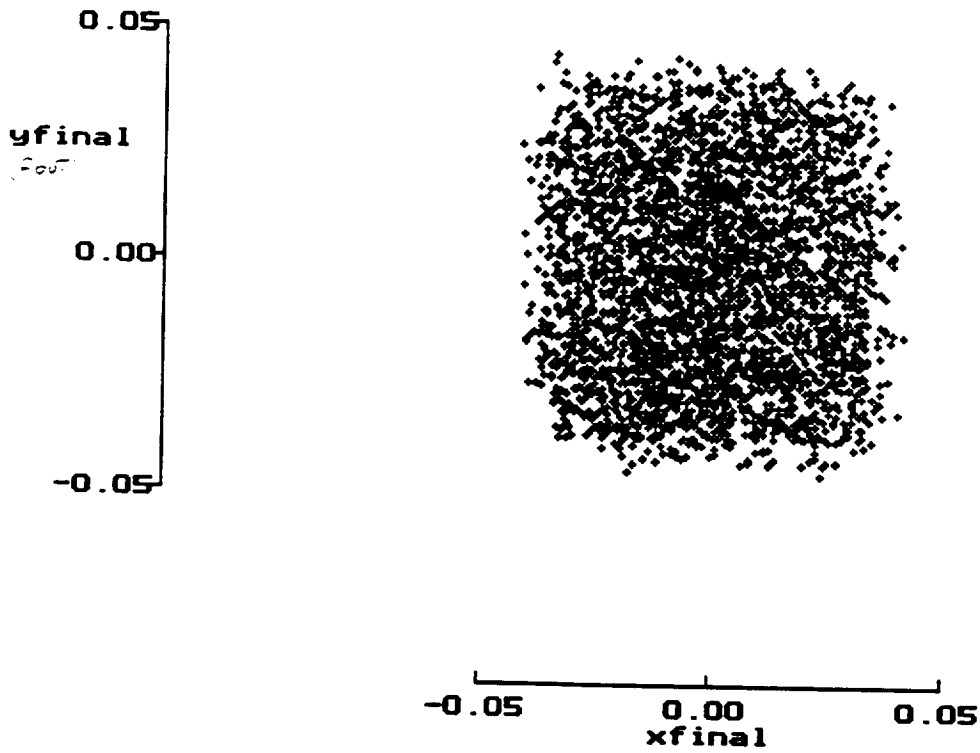


FIGURE 12: GROUP 3 FOCAL POINT IMAGE

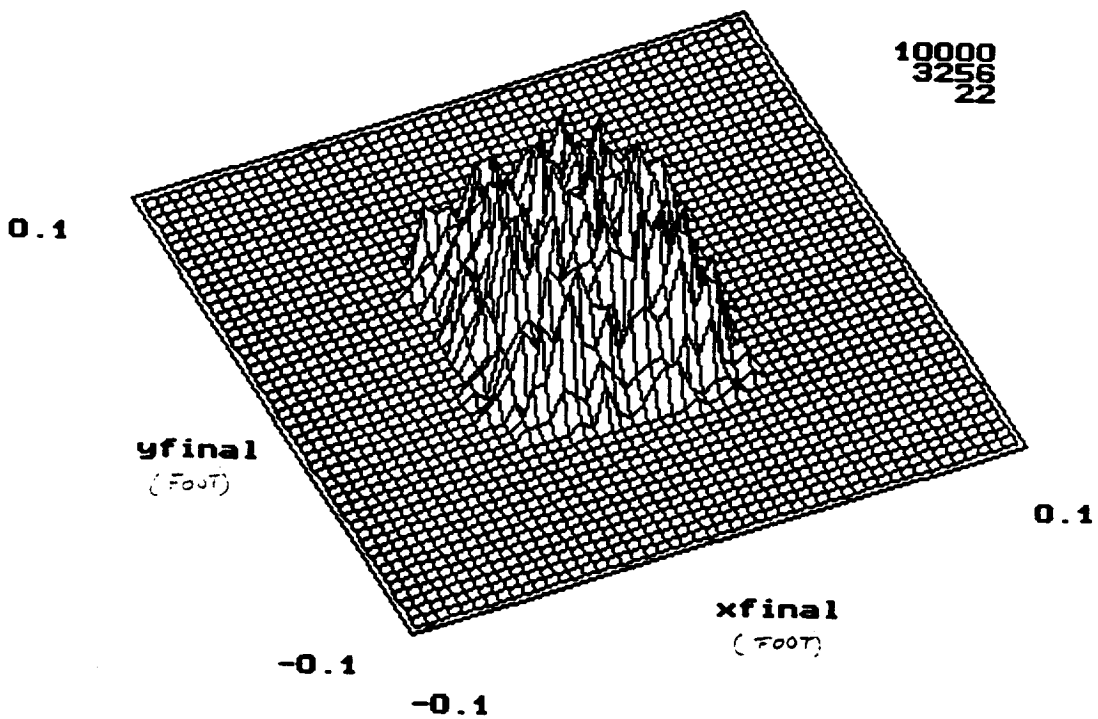


FIGURE 13: GROUP 3 FOCAL POINT 3-D INTENSITY

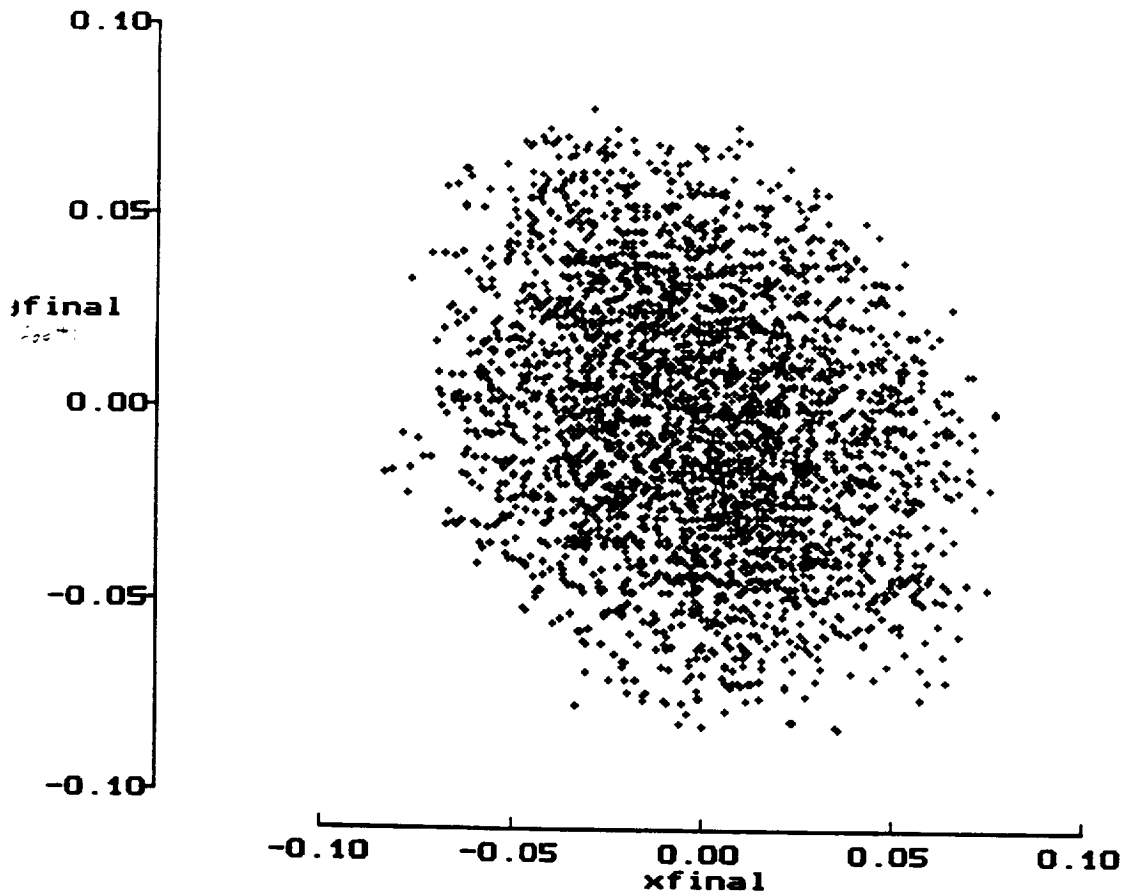


FIGURE 14: GROUP 14 FOCAL POINT IMAGE

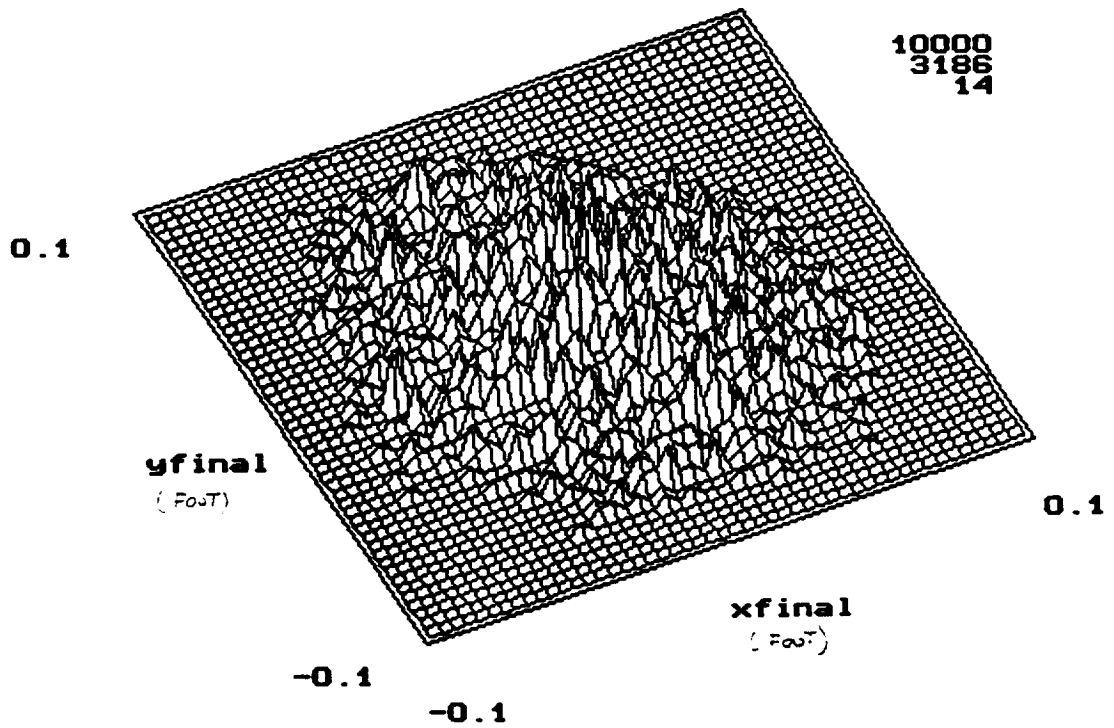


FIGURE 15: GROUP 14 FOCAL POINT 3-D INTENSITY

Apparatus Component Pictures



FIGURE 16: FACET CASTINGS



FIGURE 17: LASER MAPPING EQUIPMENT

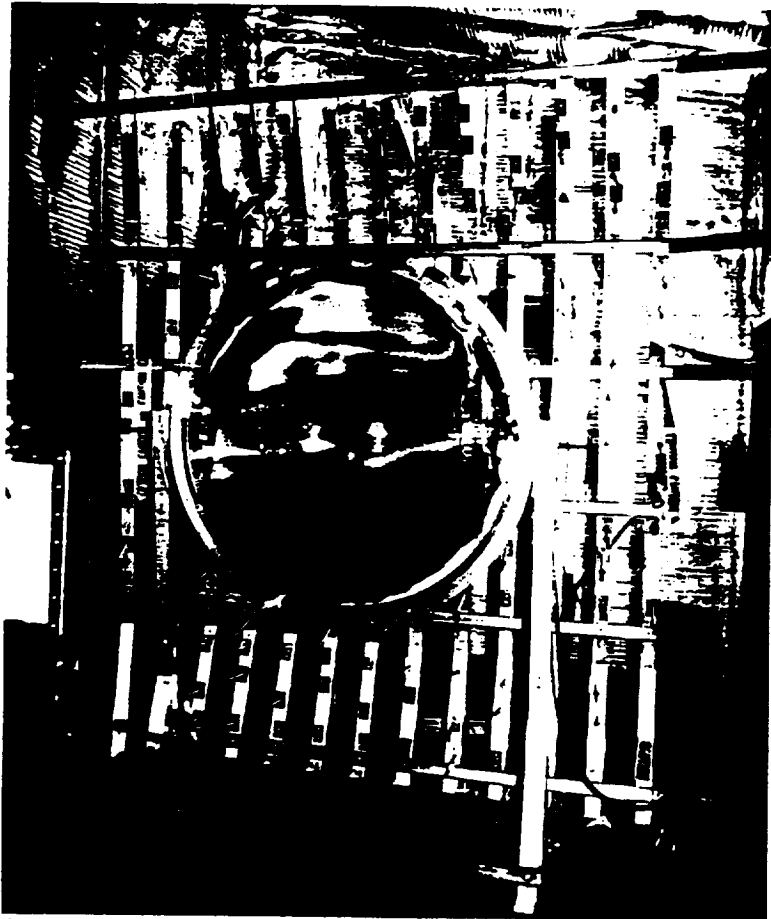


FIGURE 18: MIRROR FRAME AND SMALL MIRROR

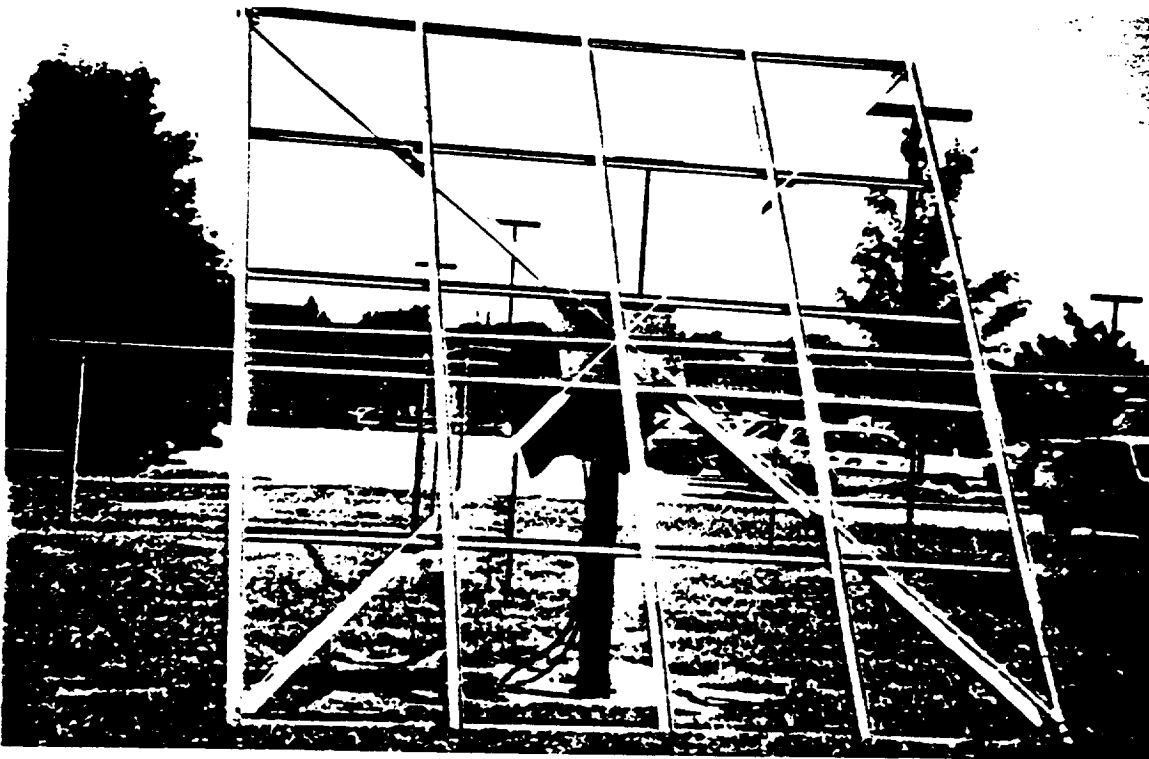
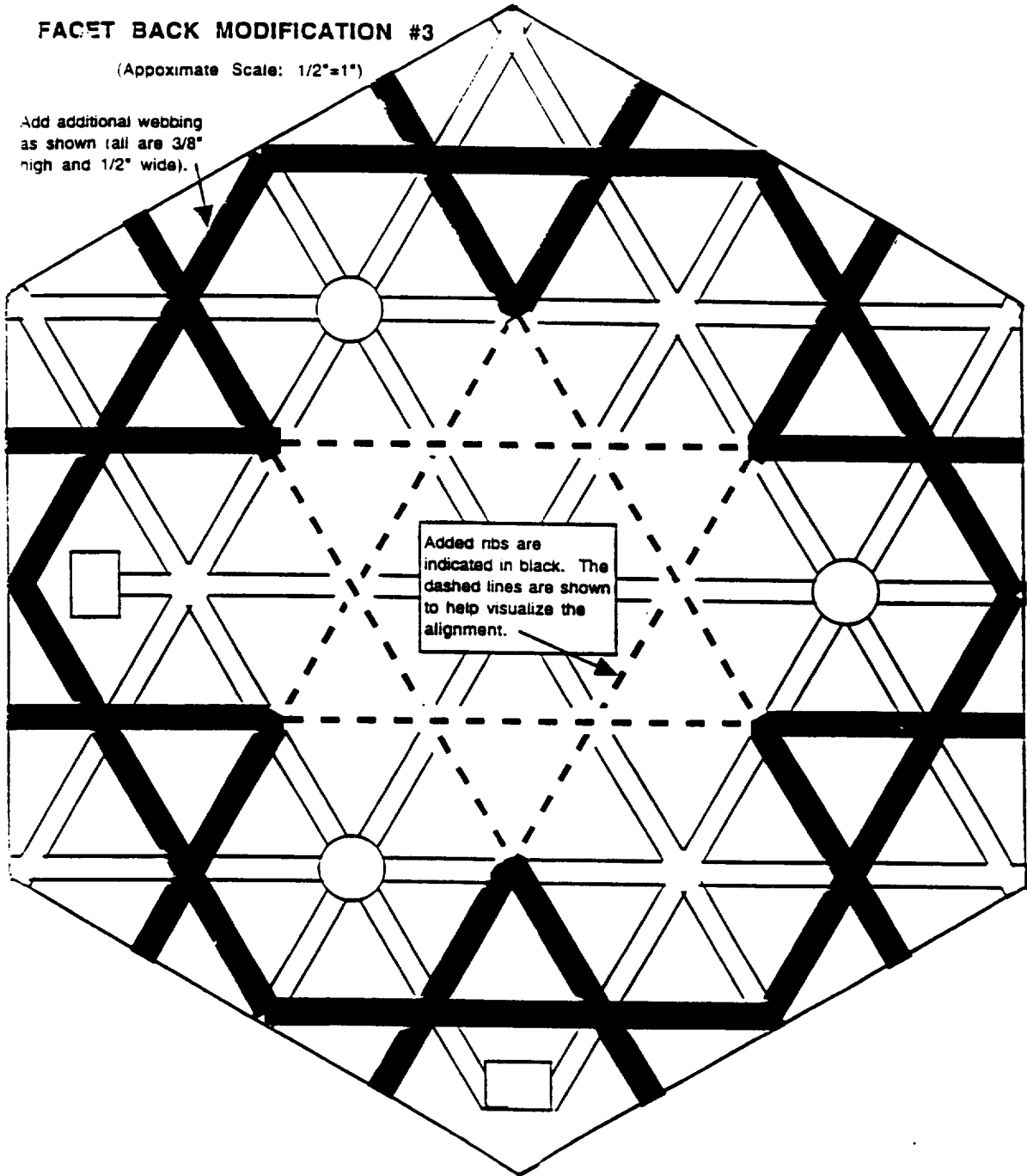


FIGURE 19: HELIOSTAT FRAME

FACET BACK MODIFICATION #3

(Approximate Scale: 1/2"=1")

Add additional webbing
as shown (all are 3/8"
high and 1/2" wide).



Added ribs are
indicated in black. The
dashed lines are shown
to help visualize the
alignment.

FIGURE 20: FACET RIB DESIGN